JOURNAL OF PETROLOGY | VOLUME 47 | NUMBER 8 | PAGES 1637–1671 | 2006 | doi:10.1093/petrology/egl023

Petrogenesis of Tertiary Mafic Alkaline Magmas in the Hocheifel, Germany

CAROLINE JUNG[1], STEFAN JUNG[1,2]*, EDGAR HOFFER[1] AND JASPER BERNDT[3]

[1]INSTITUT FÜR MINERALOGIE, PETROLOGIE UND KRISTALLOGRAPHIE, FACHBEREICH GEOWISSENSCHAFTEN, PHILIPPS UNIVERSITÄT MARBURG, LAHNBERGE/HANS-MEERWEIN-STRASSE, 35032 MARBURG, GERMANY

[2]MAX-PLANCK-INSTITUT FÜR CHEMIE, ABT. GEOCHEMIE, POSTFACH 3060, 55020 MAINZ, GERMANY

[3]INSTITUT FÜR MINERALOGIE, UNIVERSITÄT MÜNSTER, CORRENSSTR. 24, 48149 MÜNSTER, GERMANY

RECEIVED JANUARY 11, 2005; ACCEPTED MARCH 24, 2006; ADVANCE ACCESS PUBLICATION APRIL 27, 2006

Primitive nephelinites and basanites from the Tertiary Hocheifel area of Germany (part of the Central European Volcanic Province; CEVP) have high Mg-number (>0·64), high Cr and Ni contents and strong light rare earth element enrichment but systematic depletion in Rb, K and Ba relative to trace elements of similar compatibility in anhydrous mantle. Alkali basalts and more differentiated magmatic rocks have lower Mg-number and lower abundances of Ni and Cr, and have undergone fractionation of mainly olivine, clinopyroxene, Fe–Ti oxide, amphibole and plagioclase. Some nephelinites and basanites approach the Sr–Nd–Pb isotope compositions inferred for the EAR (European Asthenospheric Reservoir) component. The Nd–Sr–Pb isotope composition of the differentiated rocks indicates that assimilation of lower crustal material has modified the composition of the primary mantle-derived magmas. Rare earth element melting models can explain the petrogenesis of the most primitive mafic magmatic rocks in terms of mixing of melt fractions from an amphibole-bearing garnet peridotite source with melt fractions from an amphibole-bearing spinel peridotite source, both sources containing residual amphibole. It is inferred that amphibole was precipitated in the asthenospheric mantle beneath the Hocheifel, close to the garnet peridotite–spinel peridotite boundary, by metasomatic fluids or melts from a rising mantle diapir or plume. Melt generation with amphibole present suggests relatively low mantle potential temperatures (<1200°C); thus the mantle plume is not thermally anomalous. A comparison of recently published Ar/Ar ages for Hocheifel basanites with the geochemical and isotopic composition of samples from this study collected at the same sample sites indicates that eruption of earlier lavas with an EM signature was followed by the eruption of later lavas derived from a source with EAR or HIMU characteristics, suggesting a contribution from the advancing plume. Thus, the Hocheifel area represents an analogue for magmatism during continental rift initiation, during which interaction of a mantle plume with the overlying lithosphere may have led to the generation of partial melts from both the lower lithosphere and the asthenosphere.

KEY WORDS: *alkali basalts; continental volcanism; crustal contamination; partial melting; Eifel, Germany*

INTRODUCTION

The geochemistry of primitive, alkaline mafic volcanic rocks together with geochemical evidence from mantle-derived xenoliths can potentially yield valuable information about the nature of the inaccessible parts of the Earth's upper mantle. One problem usually addressed in studies on volcanic rocks erupted in continental areas is the identification of the source region of the alkaline magmas—either the subcontinental lithospheric mantle (SCLM) or a sublithospheric source, e.g. a mantle plume. In contrast to the suboceanic mantle, the subcontinental lithospheric mantle is likely to have remained isolated from the convecting upper mantle after initial crustal extraction. This upper mantle can have had a complex geological history, involving ancient depletion events, followed by later re-enrichments, most probably from metasomatizing fluids or melts (e.g. Hawkesworth *et al.*, 1990). The relatively large volumes of alkaline mafic magmas (nephelinites, basanites, alkali basalts) that are generated during continental rifting are often considered

*Corresponding author. Fax: ++49-6421-2828919. E-mail: jungs@staff.uni-marburg.de

to be produced predominantly by partial melting of asthenospheric mantle (McKenzie & Bickle, 1988; White & McKenzie, 1989; Wilson & Downes, 1991; Arndt & Christensen, 1992). On the other hand, there is growing evidence that, at least in some volcanic provinces, magmas are generated by partial melting of metasomatically enriched SCLM (Hawkesworth *et al.*, 1990; Gallagher & Hawkesworth, 1992; Bradshaw *et al.*, 1993). In this respect, the SCLM can contribute in several ways to the composition of continental basalts including: (1) mixing of small-degree melt fractions from the lithosphere with magmas from the asthenosphere (Ellam & Cox, 1991); (2) direct melting of the lithosphere (Bradshaw *et al.*, 1993); (3) partial melting of detached fragments of SCLM recycled into the asthenosphere during earlier tectonic episodes (Zindler & Hart, 1986).

In central Germany, several thousand km^3 of mafic magma were generated during the Tertiary and constitute part of the Central European Volcanic Province (CEVP, Fig. 1). These volumes are probably too large to have been produced solely within the lithosphere (Wedepohl, 1985; Jung & Hoernes, 1998; Jung & Masberg, 2000; Bogaard & Wörner, 2003). Consequently, it has been suggested that the individual volcanic fields of the CEVP (Massif Central, Bohemian Massif, Eifel, Siebengebirge, Westerwald, Hessian Depression, Rhön, Vogelsberg, Urach, etc.) were fed from asthenospheric partial melts generated within upwelling upper mantle plumes or diapirs (Granet *et al.*, 1995; Wilson & Patterson, 2001). The trace element and Sr–Nd–Pb isotope geochemistry of the most primitive alkaline mafic lavas from the CEPV suggest derivation from mantle sources similar to those of ocean island basalts (Wörner *et al.*, 1986; Blusztajn & Hart, 1989; Wilson & Downes, 1991; Hegner *et al.*, 1995; Wilson *et al.*, 1995; Jung & Masberg, 1998; Wedepohl & Baumann, 1999; Jung & Hoernes, 2000). Moreover, with the advent of high-resolution mantle seismic tomography, showing slow velocity domains in the mantle at various depths, an upper mantle origin for the European volcanism linked to a series of diapiric upwellings has been suggested (Granet *et al.*, 1995; Hoernle *et al.*, 1995; Goes *et al.*,

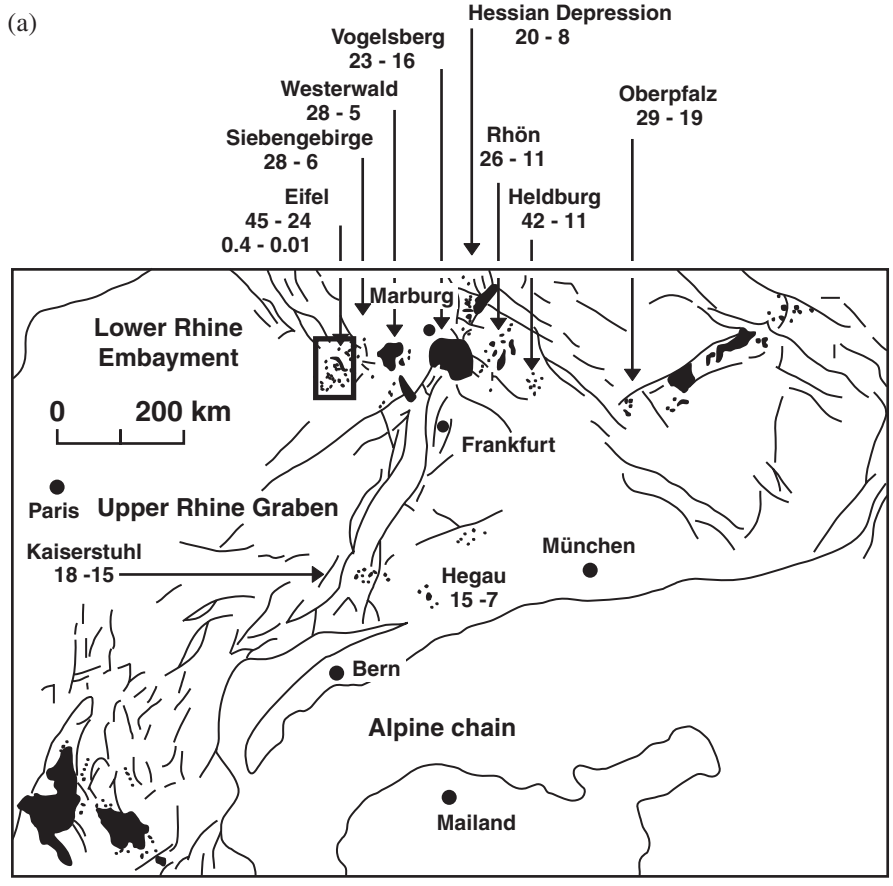

Fig. 1. (a) Distribution of Cenozoic volcanic rocks (black shaded fields) in Central Europe (modified from Wedepohl *et al.*, 1994). Numbers denote K–Ar or Ar–Ar ages compiled from Lippolt (1982) and Wilson & Downes (2006). (b) Location of the volcanic outcrops within the Hocheifel (•) with sample sites (○). Inset shows the location of the Hocheifel volcanic field relative to the east (Osteifel) and west Eifel volcanic fields.

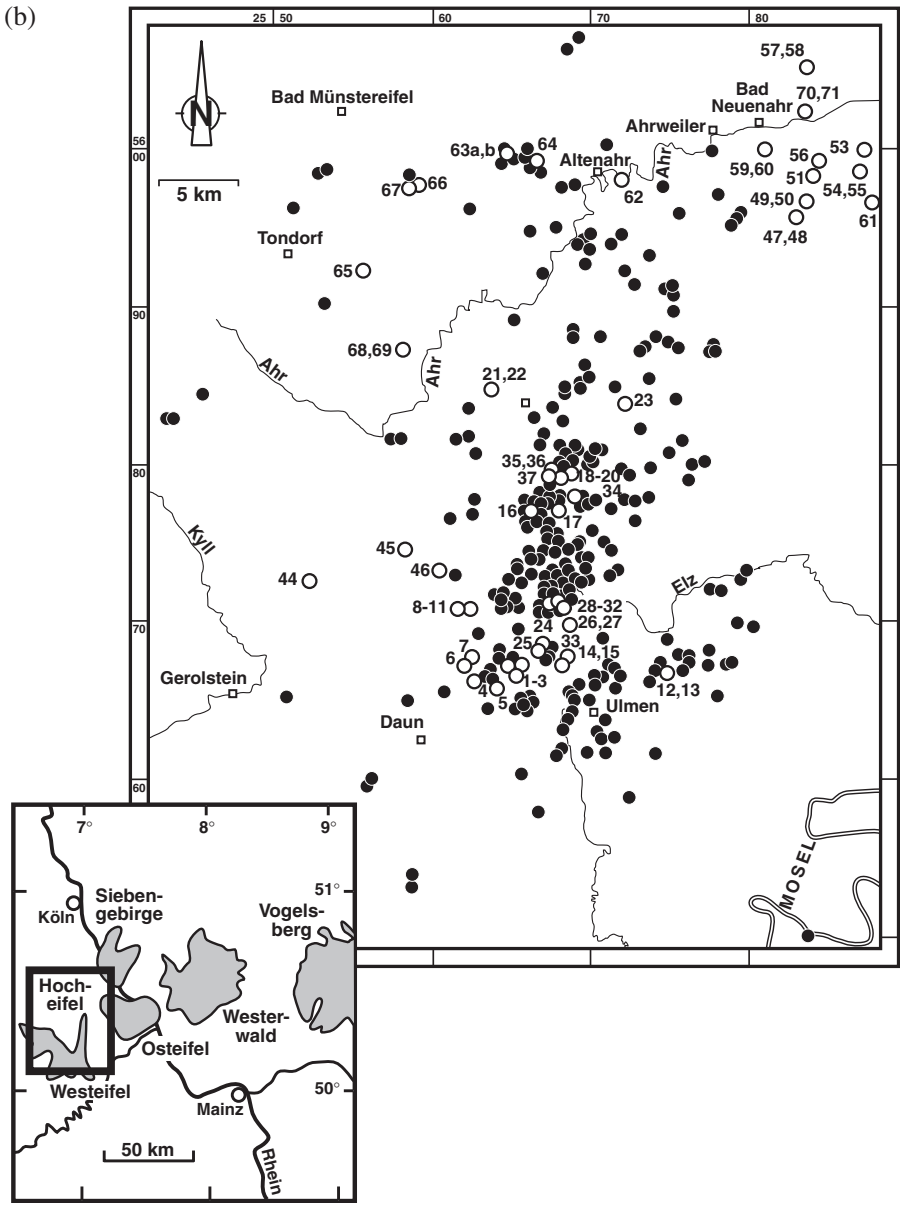

Fig. 1. Continued.

1999; Ritter *et al.*, 2001; Wilson & Patterson, 2001; Keyser *et al.*, 2002). For the Rhenish Massif, a columnar low P-wave velocity anomaly was detected beneath the Eifel (Ritter *et al.*, 2001). This 100 km wide structure extends up to 400 km depth and could be interpreted to be equivalent to an excess mantle temperature of 150–200°C in the absence of volatiles or partial melts. The geochemical diversity of lithospheric mantle xenoliths entrained within the mafic magmas of the CEPV indicates that, locally, subduction zone processes during the Hercynian orogeny may have induced substantial trace element and isotopic enrichment of the lithospheric mantle beneath central Europe (e.g. Witt-Eickschen & Kramm, 1997). Partial melting of such zones of metasomatized lithospheric mantle, combined with interaction between asthenospheric melts and lithospheric melts, has been proposed to explain the geochemical characteristics of the most primitive mafic alkaline rocks of the CEPV (Wilson & Downes, 1991; Granet *et al.*, 1995; Wilson & Patterson, 2001). In addition, crustal contamination of the mantle-derived magmas has been widely documented within the CEVP (Massif Central: Wilson *et al.*, 1995; Vogelsberg: Jung & Masberg, 1998; Bogaard & Wörner, 2003; Rhön: Jung & Hoernes, 2000; Jung *et al.*,

2006; Urach–Hegau: Blusztajn & Hegner, 2002; Westerwald: Haase *et al.*, 2004). Elucidation of the details of interaction of asthenosphere-derived melts with the lithosphere (both crust and mantle) is often difficult because both crust and ancient subcontinental mantle can have similar geochemical and Sr–Nd–Pb isotope characteristics.

Given the well-characterized nature of the crust and mantle lithosphere in the Eifel (Stosch & Lugmair, 1984, 1986; Loock *et al.*, 1990; Rudnick & Goldstein, 1990; Stosch *et al.*, 1992; Witt-Eickschen & Kramm, 1998; Witt-Eickschen *et al.*, 1998, 2003), this area provides an ideal setting in which to attempt to identify the sources of this specific type of intra-plate volcanism. However, neither comprehensive whole-rock geochemistry nor Sr–Nd–Pb isotopic data have been published for the Tertiary Hocheifel area. Such data are essential to constrain the role of fractional crystallization, crustal contamination, and mantle source heterogeneities in the petrogenesis of the magmas. In this study, major and trace element data and Sr–Nd–Pb isotope data are reported for primitive alkaline mafic magmas from the Hocheifel area; these data are used to constrain the mantle source region of these basalts. Major and trace element and Sr–Nd–Pb isotope data for more differentiated lavas from the same area are used to highlight the effects of fractional crystallization and crustal contamination in the genesis of these alkaline lavas.

GEOLOGICAL SETTING

The Hocheifel volcanic field has an areal extent of $\sim$1400 km^2 and consists mainly of deeply eroded volcanic plugs and necks. Locally, remants of lava flows appear. The Hocheifel volcanic field forms part of an east–west-trending belt of Tertiary–Quaternary volcanic fields in central Germany; these include the Eifel, Westerwald, Vogelsberg, Hessian Depression, Rhön, Heldburg and Oberpfalz (Fig. 1a). The trend of these volcanic fields is perpendicular to the main NNE–SSW-trending Rhine graben rift system of Central Europe, which has been interpreted as the result of Alpine tectonism further south (e.g. Ziegler, 1992). In Germany and elsewhere in Central Europe, Tertiary (mainly Miocene to Pliocene) basin development provides evidence for lithospheric extension, although the huge volumes of basaltic rocks in the Vogelsberg area ($\sim$500 km^3) and the Cantal (Massif Central, France) are unlikely to be attributed to continental extension alone. As noted by Wilson & Downes (1991), most of the major volcanic fields sit on uplifted Variscan basement massifs. However, basement uplift is not coeval with rift development, typically starting some 20–40 Myr after the beginning of rifting (Ziegler, 1992). Within Central Germany, although some of the Cenozoic volcanic fields are located mainly on Hercynian fault blocks within the Rhenish Massif (e.g. Eifel, Westerwald, Heldburg), Tertiary volcanic activity in the Rhön, the Hessian Depression and the Vogelsberg occurs within graben-like structures that transect the Rhenish Massif. In the Rhön area and Hessian Depression magmatism is not obviously associated with basement uplift, and dextral strike-slip movement of the lithosphere probably caused passive asthenospheric upwelling (Schreiber & Rotsch, 1998).

Geophysical data indicate that the Cenozoic rifts of the CEVP are associated with a marked uplift of the Moho discontinuity. The maximum crustal thinning coincides with the trace of the northern Rhine graben, although this area has been shown to be largely non-magmatic (Wilson & Patterson, 2001). Crustal thickness beneath the Eifel is estimated to be between 28 and 32 km (Mengel *et al.*, 1991; Prodehl *et al.*, 1992). Babuska & Plomerová (1988) estimated a lithosphere thickness of 100–140 km prior to the Cenozoic rifting and suggested a present-day depth of less than 60 km for the asthenosphere–lithosphere boundary beneath the Rhenish Massif.

Volcanism within the CEVP spans the entire Cenozoic period (Wilson & Downes, 1991); in the Hocheifel area it appears to have ranged from middle Eocene to late Oligocene (45 Ma–24 Ma; Lippolt, 1982), although new Ar–Ar data suggest a smaller age range and two distinct periods of activity (44–40 Ma and 38–34 Ma; Fekiacova *et al.* 2003). The magmatic rocks are mainly basanites, nephelinites and alkali basalts plus rare hawaiites, mugearites, benmoreites and trachytes. Volcanism in the neighbouring East and West Eifel produced about 300 small-volume monogenetic centres between 700 and 10·8 ka BP (Schmincke *et al.*, 1983; Mertes & Schminke, 1985; Wörner *et al.*, 1985). Two geochemically, spatially and temporally distinct groups of sodic–potassic alkaline volcanic rocks were erupted in the East Eifel. In the NW nephelinites, leucitites and more differentiated rocks were erupted >400 kyr ago whereas in the SE basanites and more differentiated rocks erupted between 400 and 10 ka BP. The west Eifel volcanic field consists of leucitites, basanites and nephelinites, which cover an area of $\sim$600 km^2 and erupted between 700 and 10 ka BP (Mertes & Schmincke, 1985, and references therein). Wilson & Downes (1991) suggested that the most primitive mafic alkaline volcanic rocks have major and trace element and Nd–Sr–Pb–O isotope systematics that suggest the involvement of both lithospheric and asthenospheric mantle source components in their petrogenesis. The sodic magma types (melilitites, nephelinites, basanites, alkali olivine basalts) originated by partial melting of a common asthenospheric mantle source, termed the EAR (European Asthenospheric Reservoir), whereas the potassic lavas (leucitites, leucite basanites) were derived from locally enriched portions of the mantle lithosphere. The

Hercynian basement through which the magmas erupted consists mainly of greenschist- to amphibolite-facies metapelites, metabasites and orthogneisses of the Mid German Crystalline Rise and is overlain by Palaeozoic (Lower to Upper Devonian) limestones and sandstones and Cenozoic (Triassic) sandstones, carbonates and clays (Mengel *et al.*, 1991, and references therein).

ANALYTICAL TECHNIQUES

Sixty-five samples were taken from the Hocheifel volcanic field according to the distribution of deeply eroded volcanic edifices given by Huckenholz & Büchel (1988). Based on the petrographic descriptions and average chemical compositions given by Huckenholz & Büchel (1988), a significant number of accessible sample sites were re-investigated to cover the entire range of lava compositions (Fig. 1b and Table 1). All samples were taken from remnants of lava flows, plugs and necks that cover the entire volcanic field. Whole-rock samples were prepared by crushing in an agate shatterbox to obtain ~250 g of the macroscopically freshest material. Aliquots were analysed for major and trace elements in fused lithium tetraborate glass beads using standard X-ray fluorescence (XRF) techniques (Vogel & Kuipers, 1987) at the Mineralogical–Petrological Department at the University of Bonn. Rare earth elements (REE) were analysed by inductively coupled plasma atomic emission spectrometry (ICP-AES) following separation of the matrix elements by ion exchange (Heinrichs & Herrmann, 1990) at the Department of Mineralogy, Petrology and Crystallography at the University of Marburg. Loss on ignition (LOI) was determined gravimetrically at 1050°C (Lechler & Desilets, 1987) and FeO was measured titrimetrically using standard techniques. Accuracy was monitored by repeated measurements of international and in-house standards; the results are in good agreement with the recommended values for the international rock standard JB 2 given by Govindaraju (1994) (Table 2).

Pb, Sr and Nd isotope analyses were carried out at the Max-Planck-Institut für Chemie at Mainz by thermal ionization mass spectrometry using a Finnigan MAT 261 multiple sample, multicollector mass spectrometer operating in the static mode. Whole-rock chips were leached in 6N HCl for at least 2 h on a hotplate. Subsequently, the samples were washed three times with ultrapure H_2O. After this treatment, the samples were dissolved in concentrated HF and after evaporation redissolved in 2·5N HCl and 0·6N HBr and loaded on Teflon® columns filled with DOWEX® AG 1×8 anion exchange resin (100–200 mesh) in chloride form (Mattinson, 1986). The Pb was extracted using conventional HBr–HCl techniques and was loaded on Re single filaments following the H_3PO_4–silica gel method (Cameron *et al.*, 1969). Strontium and REE were separated by using standard cation exchange columns with a DOWEX® AG 50 W-X 12 resin using 2·5N HCl for Sr and 6N HCl for the REE. Nd was separated from the other REE by using HDEHP-coated Teflon® columns and 0·12N HCl. Neodymium isotopes were normalized to $^{146}Nd/^{144}Nd = 0{\cdot}7219$. Repeated measurements of the La Jolla Nd standard gave $^{143}Nd/^{144}Nd = 0{\cdot}511848 \pm 0{\cdot}000021$ (2σ; $n = 28$). The reproducibilitiy of the Sr standard (NBS 987) is $^{87}Sr/^{86}Sr = 0{\cdot}710224 \pm 0{\cdot}000024$ (2σ; $n = 14$) and the fractionation was corrected to $^{86}Sr/^{88}Sr = 0{\cdot}1194$. Lead analyses were corrected for mass fractionation by a factor of 0·11% per a.m.u. The reproducibility of the standard NBS 982 was estimated to be 0·068%, 0·064% and 0·071% for the $^{206}Pb/^{204}Pb$, $^{207}Pb/^{204}Pb$ and $^{208}Pb/^{204}Pb$ ratio, respectively. The total procedure blank is <60 pg Pb during this study and is therefore considered negligible.

PETROGRAPHY

All samples are porphyritic and contain partly altered olivine and clinopyroxene phenocrysts. Usually, the majority of the olivine and clinopyroxene phenocrysts have grain sizes of ~1–2 mm and 0·5–5 mm, respectively, and the samples containing such phenocrysts do not appear to be accumulative. Rare olivines in some basanites and nephelinites have a mosaic texture and incipient undulose extinction. They probably represent entrained material from disintegrated peridotite xenoliths. Chemically, these olivines appear to be enriched in MgO and depleted in FeO relative to the dominant euhedral olivines (Table 2). The dominant olivines within the nephelinites and basanites are euhedral phenocrysts with sharply defined crystal edges. Sometimes, the olivines are more skeletal with evidence of marginal resorption, re-entrants and internal cavities. These olivines have slightly lower MgO but higher FeO than the olivines, with incipient undulose extinction (Table 2). Both types of olivine show a narrow rim with depletion of MgO and enrichment of FeO.

Zoned clinopyroxenes are generally composed of a subhedral to anhedral colourless to pale brown core and a darker brown, slightly pleochroic mantle. The core of these clinopyroxenes is usually more MgO-poor and FeO-rich than the rim (Table 2). The evolution of clinopyroxene in the sequence basanite–mugearite–tephrite shows increasing MgO but decreasing FeO, suggesting a complex pre-eruption history (Fig. 2a). In some samples, clinopyroxenes with an olive green to light green core, a colourless to pale brown mantle and a dark brown rim occur in addition to the clinopyroxenes described above. The green core of these clinopyroxene is enriched

Table 1: Sample localities and petrographic characteristics

Sample	Location	Description	Easting	Northing
HEJ 1	Gefell West	Fine-grained tephrite, <5% phen of cpx, amph, abundant green-core cpx and crustal xenoliths	256462	556736
HEJ 2	Gefell West	Fine-grained basanite, <10% phen of cpx and ol, abundant green-core cpx	256480	556735
HEJ 3	Gefell West	Fine-grained basanite, <10% phen of cpx and ol, abundant green-core cpx and amphibole	256480	556735
HEJ 4	Kapp	Fine-grained basanite, <5% phen of ol, rare green-core cpx	256366	556646
HEJ 5	Ehlert	Fine-grained nephelinite, <10% phen of ol and cpx, abundant green-core cpx, rare altered amph	256369	556600
HEJ 6	Roadcut Samersbach–Nerdlen	Fine-grained basanite, <10% phen of cpx and ol, abundant glomerophyric clots of cpx	256192	556735
HEJ 7	Roadcut Samersbach–Nerdlen	Fine-grained basanite, <5% phen of cpx and ol, altered crustal xenoliths	256214	556766
HEJ 8	Neicher Berg	Fine-grained alkali basalt, <10% phen of cpx, rare skeletal ol	256400	557150
HEJ 9	Neicher Berg	Fine-grained basanite, <15% phen of cpx and ol, green-core cpx, individual cpx and ol phen >5 mm	256400	557150
HEJ 10	Neicher Berg	Fine-grained mugearite, <15% phen of cpx and plag, altered amph	256400	557150
HEJ 11	Neicher Berg	Fine-grained benmoreite, <15% phen of plag, rare cpx and altered amph	256400	557150
HEJ 13	Höchstberg Süd	Fine-grained basanite, <5% ol phen, abundant ol xenocrysts	256810	556747
HEJ 14	Kastelberg	Fine-grained nephelinite, <15% phen of cpx and ol, rare green-core cpx	256662	557710
HEJ 16	Scharfer Kopf	Fine-grained basanite, <15% phen of cpx and ol, rare green-core cpx	256760	557950
HEJ 17	Bränkekopf	Fine-grained basanite, <10% phen of cpx and ol, rare green-core cpx, ol often skeletal and altered	256750	557950
HEJ 18	Nürburg W	Fine-grained nephelinite, <10% phen of ol, rare cpx	256800	557940
HEJ 19	Nürburg S	Fine-grained nephelinite, <10% phen of ol, rare cpx	256845	557970
HEJ 20	Steinchen	Fine-grained alkali basalt, <10% cpx phen, rare ol phen, flow texture	256345	558488
HEJ 21	Alte Burg/Reiferscheid	Fine-grained basanite, <10% cpx and ol phen, large phen (≤1·5 cm) of amph, amph slightly altered	256345	558488
HEJ 22	Alte Burg/Reiferscheid	Fine-grained basanite, <10% cpx and ol phen, large phen (≤1·5 cm) of amph, amph slightly altered	256345	558488
HEJ 23	Hohe Acht	Fine-grained basanite, <15% phen of cpx and ol	257080	258250
HEJ 25	Roadcut Horperath–Ueß	Fine-grained hawaiite, <15% phen of cpx and amph, tiny laths of plag	256750	556850
HEJ 26	Bittberg	Fine-grained nephelinite, <10% phen of ol, rare cpx, some xenocrystic ol	256900	556950
HEJ 27	Bittberg	Fine-grained nephelinite, <10% phen of ol, rare cpx, some xenocrystic ol	256900	556950
HEJ 28	Hochkehlberg	Fine-grained nephelinite, <15% phen of ol and cpx, some xenocrystic ol, rare green-core cpx	256800	557136
HEJ 29	Hochkehlberg	Fine-grained benmoreite, <20 % phen of cpx and amph, abundant plg	256715	557176
HEJ 30	Hochkehlberg	Fine-grained nephelinite, <10% phen of ol, rare cpx, some xenocrystic ol	256800	557136
HEJ 31	Hochkehlberg	Fine-grained nephelinite, <10% phen of ol, rare cpx, some xenocrystic ol	256800	557136
HEJ 32	Hochkehlberg	Fine-grained basanite, <10% phen of ol, rare cpx, some xenocrystic ol	256830	557127
HEJ 33	Simonsberg	Fine-grained basanite, <10% phen of ol and cpx	256590	556950
HEJ 34	Krebsberg	Fine-grained basanite, <5% phen of ol, abundant microphen of cpx, ol often skeletal	256810	557900

Sample	Location	Description	Easting	Northing
HEJ 35	W'In der Stroth (close to Nürburg)	Fine-grained hawaiite, <5% phen of cpx, abundant plg	256820	557950
HEJ 37	Selberg	Fine-grained tephriphonolite, <10% phen of cpx and amph, abundant plg,, flow texture	256734	557900
HEJ 44	Arensberg	Fine-grained basanite, <5% phen of ol and cpx, abundant microphen of cpx, ol skeletal, large green-core cpx	255200	557250
HEJ 45	Heyer Berg	Fine-grained basanite, <5% phen of ol and cpx	255800	557450
HEJ 46	Barsberg	Fine-grained basanite, <10% phen of ol and cpx, green-core cpx, ol often skeletal	256000	557270
HEJ 47	Steinberg am Königssee	Fine-grained basanite, <20% phen of ol and cpx, large cpx often corroded	258200	559500
HEJ 48	Steinberg am Königssee	Fine-grained basanite, <20% phen of ol and cpx, large cpx often corroded	258200	559500
HEJ 49	Steinebüchelchen near Königsfeld	Fine-grained nephelinite, <15% phen of ol and cpx, abundant glomerophyric clots of cpx	258300	559560
HEJ 50	Steinebüchelchen near Königsfeld	Fine-grained nephelinite, <15% phen of ol and cpx, green-core cpx	258283	559554
HEJ 51	Kirchberg bei Königsfeld	Fine-grained nephelinite, <10% phen of ol and cpx, rare green-core cpx, ol often skeletal	258400	559700
HEJ 53	Sinzigkopf	Fine-grained alkali basalt, <10% cpx, rare olivine and green-core cpx, abundant laths of plg	256850	559850
HEJ 54	Hombüchel	Fine-grained basanite, <10% phen of ol and cpx, cpx often corroded, peridotite xenoliths, rare green-core cpx	256850	559800
HEJ 55	Hombüchel	Fine-grained basanite, <10% phen of ol and cpx, large cpx often corroded, peridotite xenoliths	256850	559800
HEJ 56	Steinberg near Schloß Vehn	Fine-grained basanite, <10% phen of ol and cpx, green-core cpx, peridotite xenoliths	258400	559850
HEJ 57	Scheidskopf near Kirchdaun	Fine-grained basanite, <15% phen of ol and cpx	258270	560450
HEJ 58	Scheidskopf near Kirchdaun	Fine-grained basanite, <15% phen of ol and cpx, ol slightly altered, peridotite xenoliths	258270	560450
HEJ 59	Neuenahrer Burgberg	Fine-grained nephelinite, <15% phen of ol and cpx, ol often skeletal, green-core cpx, crustal xenoliths	258070	560010
HEJ 60	Neuenahrer Burgberg	Fine-grained nephelinite, <15% phen of ol and cpx, ol often skeletal, green-core cpx, abundant il	258070	560010
HEJ 61	Steinbergskopf near Niederlützingen	Fine-grained alkali basalt, <15% ol and cpx, abundant laths of plg, rare green-core cpx	259150	559410
HEJ 62	Lochmühle bei Maischoß	Fine-grained basanite, <15% cpx, rare ol phen, rare vesicles	257380	559800
HEJ 63 a	Hochthürmen	Fine-grained basanite, <15% phen of ol and cpx, green-core cpx, ol slightly altered	256430	559950
HEJ 63 b	Hochthürmen	Fine-grained basanite, <15% phen of ol and cpx, rare green-core cpx	256430	559950
HEJ 64	Hasenberg	Fine-grained basanite, <15% phen of ol and cpx, ol slightly altered, large cpx often corroded	256640	559930
HEJ 66	Michelsberg Mitte	Fine-grained basanite, <15% phen of ol and cpx, ol slightly altered, large cpx often corroded	255820	559750
HEJ 67	Michelsberg Süd	Fine-grained nephelinite, <10% phen of ol and cpx, ol often skeletal, green core cpx, peridotite xenoliths	255810	559740
HEJ 68	Aremberg	Fine-grained basanite, <15% phen of ol and cpx, large phen of cpx often corroded, large phen of altered amph	255800	558650
HEJ 70	Landskrone near Lohrsdorf	Fine-grained basanite, <10% phen of ol and cpx, ol slightly altered	258250	560220
HEJ 71	Landskrone near Lohrsdorf	Fine-grained alkali basalt, <10% phen ol and cpx, abundant laths of plg, rare green-core cpx	258250	560220

Geographical information based on the German (Gauss–Krüger) coordinate system. Sample locations are shown in Fig. 1. phen, phenocryst; ol, olivine; cpx, clinopyroxene; amph, amphibole; plg, plagioclase; il, ilmenite.

Table 2: Representative clinopyroxene, amphibole, plagioclase and olivine composition from Hocheifel basalts

	Cpx HEJ 21		Cpx HEJ 10		Cpx HEJ 12 (green-core Cpx)			Cpx HEJ 1	
	core	rim	core	rim	core	rim	outermost rim	core	rim
SiO_2	46·12	43·02	45·25	45·82	43·52	44·88	48·22	47·82	43·79
TiO_2	2·18	3·59	2·35	2·37	3·00	2·67	1·75	1·91	2·43
Al_2O_3	8·48	11·47	8·29	8·88	10·72	9·16	7·09	6·81	9·63
FeO	9·91	8·02	9·14	9·00	10·97	6·28	5·74	8·42	12·04
MnO	0·18	0·20	0·19	0·32	0·30	0·09	0·08	0·18	0·35
MgO	10·28	10·87	10·96	11·06	8·29	12·79	13·16	11·99	8·11
CaO	22·02	23·23	22·56	22·51	21·68	22·97	22·94	22·85	21·83
Na_2O	0·96	0·51	0·72	0·72	1·34	0·49	0·46	0·70	1·22
K_2O	0·01	0·02	0·01	0·02	0·08	0·00	0·01	0·00	0·01
Total	100·13	100·91	99·46	100·70	99·90	99·34	99·44	100·67	99·41

	Amph HEJ 21		Amph HEJ 10		Amph HEJ 1		Plag HEJ 10		
	core	rim	core	rim	core	rim	core	rim	outermost rim
SiO_2	39·47	40·46	39·04	38·85	40·23	40·23	57·71	52·71	67·00
TiO_2	4·22	4·21	4·70	4·85	4·41	4·44	0·08	0·02	0·04
Al_2O_3	15·11	15·02	14·69	14·46	13·49	13·71	27·08	29·46	18·91
FeO	9·99	10·05	11·49	11·46	12·51	12·81	0·33	0·54	0·42
MnO	0·01	0·12	0·11	0·20	0·20	0·19	0·02	0·01	0·00
MgO	13·79	13·63	12·28	12·21	11·32	11·30	0·01	0·03	0·03
CaO	12·18	12·00	12·26	12·01	12·04	11·82	9·45	12·29	0·98
Na_2O	2·38	2·56	2·65	2·56	2·72	2·61	5·70	4·34	5·70
K_2O	1·46	1·39	1·10	1·05	1·26	1·19	0·50	0·27	7·06
Total	98·61	99·44	98·32	97·65	98·18	98·30	100·88	99·67	100·13

	Olivine HEJ 26 (xenocryst)		Olivine HEJ 26(phenocryst)	
	core	rim	core	rim
SiO_2	39·57	39·19	39·01	39·26
TiO_2	0·00	0·02	0·03	0·01
Al_2O_3	0·06	0·03	0·06	0·03
FeO	11·35	20·92	17·95	22·70
MnO	0·20	0·45	0·27	0·70
MgO	48·89	39·70	42·80	38·58
CaO	0·19	0·43	0·21	0·38
Na_2O	0·02	0·02	0·00	0·00
K_2O	0·01	0·00	0·01	0·02
Total	100·30	100·75	100·33	101·67

in FeO and Al_2O_3 and depleted in MgO. Whereas the core is unzoned, the pale brown mantle shows increasing MgO starting at a much higher MgO content. This evolution is followed by a decrease in MgO and a narrow zone of MgO enrichment when approaching the rim. In this sequence, FeO, Al_2O_3 and TiO first decrease and then increase through the mantle. Towards the outermost rim, the composition of the clinopyroxene shows a complex evolution of generally increasing Al_2O_3, FeO and TiO_2, starting at lower values than the mantle values, whereas MgO decreases towards the outermost rim (Fig. 2a).

The mostly euhedral form of some of the green cores suggests that they crystallized from a melt. This melt must have been more differentiated than the host basanite because of the lower MgO but higher Al_2O_3, FeO and TiO_2 abundances. On the other hand, the chemical characteristics of the mantles suggest that they crystallized from a more mafic magma (higher MgO, lower Al_2O_3, FeO and TiO_2). The outermost rims of the green-core cpx vary according to normal low-pressure fractionation trends (e.g. increasing Ti, Al and Fe, and decreasing Mg). These features are characteristics of clinopyroxene crystallizing from an alkali basaltic magma (e.g. Duda & Schmincke, 1985). The development of the more primitive mantles around the more evolved cores can be attributed to mixtures of the host basanitic melt with evolved (?tephritic) melts stored in the mantle, which resulted from earlier episodes of magma generation and fractionation. Mixing between evolved and primitive melts, believed to be associated with magma replenishment (e.g. Huppert & Sparks, 1988), can account for the progression from evolved cores towards mafic rims of the clinopyroxene phenocrysts.

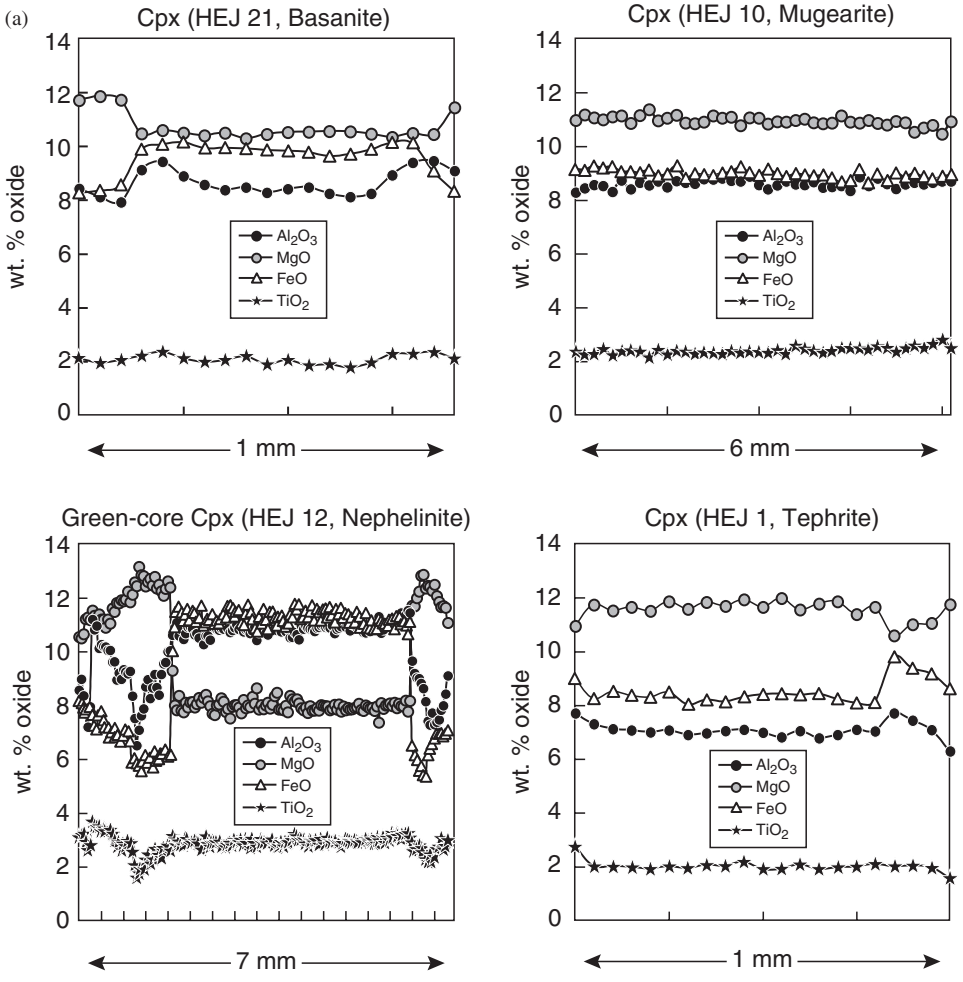

Fig. 2. (a) Representative clinopyroxene compositional profiles from samples HEJ 21 (basanite), HEJ 10 (mugearite), HEJ 12 (nephelinite) and HEJ 1 (tephrite); (b) representative amphibole compositional profiles from samples HEJ 21, HEJ 10 and HEJ 1, and a plagioclase compositional profile from sample HEJ 10.

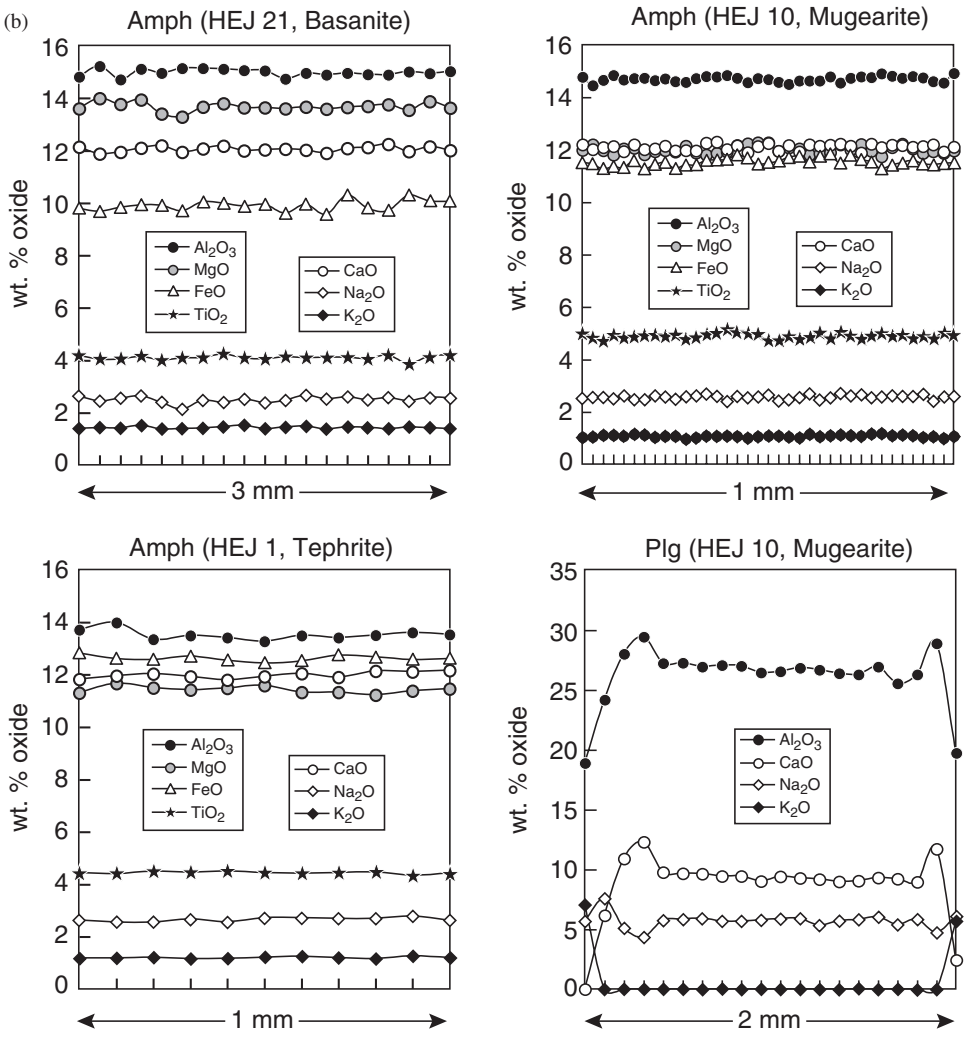

Fig. 2. Continued.

Therefore, the crystallization scenario shown by the different clinopyroxene types suggests discrete storage zones for the alkali basaltic magmas.

Some basanites and some of the more differentiated rocks contain optically homogeneous, unzoned brown amphibole (kaersutite) phenocrysts with a grain size between 1 mm and 2 cm (Table 2 and Fig. 2b). Plagioclase is common only in some alkali basalts and in the more differentiated rocks and is generally unzoned (Table 2). Rare large plagioclase crystals show the development of K-feldspar-rich rims (Fig. 2b).

GEOCHEMISTRY

Chemical composition of the Hocheifel lavas

The mafic magmatic rocks from the Hocheifel area are mostly relatively primitive basanites, nephelinites and alkali basalts with rare hawaiites, mugearites and benmoreites, according to the total-alkali vs SiO_2 classification sheme of Le Bas *et al.* (1986) (Table 3; Fig. 3a). According to the classification proposed by Huckenholz & Büchel (1986) and Le Bas (1989), samples with >10% normative nepheline, $CaO + Na_2O + K_2O < 18$ at $SiO_2 + Al_2O_3 < 55$ and <41 wt % SiO_2 are classified as nephelinites. For the nephelinites and basanites, TiO_2, MgO, CaO and $FeO_{(total)}$ decrease and K_2O and Al_2O_3 increase with increasing SiO_2 (Fig. 3). Na_2O (not shown) shows considerable scatter among the nephelinites and basanites but generally increases with increasing SiO_2. For the evolved rocks (hawaiites, mugearites and benmoreites), TiO_2, MgO, CaO and FeO decrease with increasing SiO_2, whereas K_2O, Al_2O_3 and Na_2O increase (Fig. 3). P_2O_5 decreases from nephelinites to alkali basalts but increases with increasing SiO_2 in the more differentiated rocks. Basanites and nephelinites

Table 3: Chemical composition of Hocheifel lavas

	Neph. HEJ 5	Neph. HEJ 18	Neph. HEJ 19	Neph. HEJ 49	Neph. HEJ 50	Neph. HEJ 51	Neph. HEJ 59	Neph. HEJ 60	Neph. HEJ 67	Neph. HEJ 26	Neph. HEJ 27	Neph. HEJ 28
SiO_2	40·81	40·68	40·77	40·94	40·90	40·99	40·93	40·65	40·47	41·02	40·79	40·52
TiO_2	2·48	2·43	2·52	2·52	2·52	2·50	2·44	2·37	2·55	2·41	2·36	2·48
Al_2O_3	12·33	13·01	13·07	13·25	13·17	13·16	13·38	13·30	13·13	11·48	11·28	11·56
Fe_2O_3	5·02	4·53	4·56	4·81	5·14	4·84	5·01	5·01	4·92	4·79	3·90	4·00
FeO	6·65	6·46	6·78	6·29	5·98	6·18	5·62	5·35	6·47	7·13	7·70	7·87
MnO	0·17	0·17	0·17	0·16	0·17	0·16	0·15	0·15	0·17	0·18	0·17	0·17
MgO	13·22	11·31	11·45	11·40	11·41	10·84	11·65	11·26	11·05	13·94	14·30	14·03
CaO	11·72	12·79	13·20	12·49	12·52	12·73	12·53	12·32	12·97	12·61	12·81	12·76
Na_2O	2·87	3·34	3·49	3·57	3·67	3·79	3·19	3·31	3·52	2·80	2·09	2·50
K_2O	1·03	0·89	0·80	0·91	0·94	0·91	1·09	1·06	0·94	0·74	0·68	0·88
P_2O_5	0·65	0·73	0·75	0·69	0·69	0·69	0·77	0·73	0·81	1·20	1·17	1·12
LOI	2·05	2·24	2·17	2·50	2·46	2·87	3·12	3·55	2·08	2·33	3·68	2·65
Total	99·00	98·58	99·73	99·53	99·57	99·66	99·88	99·06	99·08	100·63	100·93	100·54
Mg-no.	69	67	67	67	67	66	68	68	66	70	71	70
Sc	23	27	16	11	23	19	26	11	12	23	11	16
V	286	297	310	308	315	307	312	303	319	281	283	292
Cr	399	379	351	335	340	331	383	361	288	562	556	583
Co	63	57	52	42	50	42	54	49	44	65	69	61
Ni	354	194	189	181	188	179	213	212	177	373	407	363
Cu	52	62	58	53	66	66	85	73	67	51	57	70
Zn	92	88	91	91	89	83	84	86	88	98	98	98
Ga	18	18	16	27	19	14	20	20	17	25	19	17
Rb	36	46	44	41	33	40	33	44	48	28	32	23
Sr	819	904	1162	879	881	906	944	947	995	1084	1160	1060
Y	34	28	35	29	31	34	30	26	30	34	35	31
Zr	259	278	276	264	263	263	239	226	271	277	274	271
Nb	96	92	95	93	90	90	88	84	98	94	90	84
Ba	526	649	618	727	729	713	710	697	755	620	649	569
La	65·6	71·7	73·1	72·9	63·4	68·3	70·4	67·2	78·5	81·4	75·8	80·2
Ce	131·9	140·8	137·1	141·4	129·3	132·9	141·3	135·0	138·9	166·1	138·4	165·9
Nd	54·9	50·4	51·0	53·6	50·1	55·2	52·6	46·4	60·9	67·0	58·3	60·6
Sm	12·2	10·1	11·7	11·4	9·40	10·7	9·80	10·1	10·9	12·6	12·1	12·1
Eu	2·92	2·80	2·84	2·91	2·53	2·88	2·56	2·44	2·83	3·23	2·89	3·37
Gd	9·05	7·41	7·62	7·25	6·36	7·28	6·45	6·86	7·78	9·01	7·45	8·89
Dy	6·55	6·08	6·17	5·88	5·54	6·51	5·63	5·30	6·74	6·51	5·69	6·81
Er	2·83	2·80	2·60	2·80	2·53	2·78	2·74	2·70	3·16	2·53	2·44	2·72
Yb	2·45	2·29	2·19	2·32	2·17	2·31	2·29	2·20	2·43	2·27	2·08	2·15
Lu	0·33	0·33	0·28	0·30	0·31	0·32	0·3	0·31	0·35	0·29	0·29	0·29

	Neph. HEJ 30	Neph. HEJ 31	Neph. HEJ 32	Neph. HEJ 24	Bas. HEJ 2	Bas. HEJ 3	Bas. HEJ 66	Bas. HEJ 34	Bas. HEJ 46	Bas. HEJ 4	Bas. HEJ 6	Bas. HEJ 7	Bas. HEJ 16	Bas. HEJ 17
SiO_2	40·82	40·83	40·04	40·70	42·48	42·84	42·12	41·46	41·95	41·11	44·65	42·30	44·85	44·41
TiO_2	2·47	2·18	2·20	2·84	2·32	2·32	2·44	2·48	2·63	2·34	1·98	2·32	2·24	2·24
Al_2O_3	11·56	10·48	10·45	11·14	13·18	13·41	13·05	13·18	14·02	12·40	13·62	13·54	13·67	13·57
Fe_2O_3	6·85	4·44	4·46	6·45	4·41	4·04	4·99	4·72	4·37	3·85	3·58	4·05	4·32	4·91

Table 3: continued

	Neph. HEJ 30	Neph. HEJ 31	Neph. HEJ 32	Neph. HEJ 24	Bas. HEJ 2	Bas. HEJ 3	Bas. HEJ 66	Bas. HEJ 34	Bas. HEJ 46	Bas. HEJ 4	Bas. HEJ 6	Bas. HEJ 7	Bas. HEJ 16	Bas. HEJ 17
FeO	5·36	7·41	7·44	4·16	6·40	6·54	6·17	6·41	6·61	7·11	6·68	5·94	6·72	6·12
MnO	0·17	0·18	0·17	0·13	0·16	0·17	0·17	0·17	0·16	0·16	0·14	0·15	0·15	0·14
MgO	14·07	16·30	16·91	10·05	11·82	11·47	10·73	11·66	11·18	13·24	11·17	11·15	9·26	9·11
CaO	12·56	11·51	11·53	10·66	11·77	11·72	12·53	13·03	12·18	11·55	9·66	12·07	11·60	11·62
Na_2O	2·68	2·50	2·65	1·16	2·91	2·84	3·42	3·44	3·50	2·59	3·19	3·23	3·44	2·92
K_2O	0·76	0·68	0·58	1·34	0·94	0·91	1·05	1·37	1·40	0·71	1·35	0·92	1·14	0·80
P_2O_5	1·16	1·21	1·22	0·69	0·66	0·67	0·77	0·74	0·61	0·60	0·44	0·59	0·64	0·66
LOI	2·06	2·33	2·27	11·20	2·30	2·57	2·34	1·85	1·85	3·54	2·06	2·73	1·37	2·83
Total	100·52	100·05	99·92	100·52	99·35	99·50	99·78	100·51	100·46	99·20	98·52	98·99	99·40	99·33
Mg-no.	70	73	74	66	68	68	66	67	67	70	68	69	62	62
Sc	22	16	27	26	20	16	25	34	28	25	24	30	20	23
V	238	254	244	302	269	282	301	320	302	285	229	277	244	255
Cr	607	704	698	225	368	346	306	387	267	444	305	467	347	367
Co	65	74	65	46	59	54	52	51	56	62	51	54	45	47
Ni	366	531	548	167	235	224	180	200	169	319	280	215	177	179
Cu	47	50	50	61	61	44	78	57	65	53	50	68	61	57
Zn	103	101	106	106	99	90	94	88	92	88	99	78	94	95
Ga	12	11	15	19	23	15	19	23	21	18	20	18	25	17
Rb	22	34	30	31	39	25	51	52	37	49	36	61	27	17
Sr	1034	1013	1062	1041	943	942	940	889	910	1015	754	739	881	879
Y	33	31	33	37	25	33	34	32	28	29	29	30	27	29
Zr	281	268	272	245	260	260	262	274	275	250	245	231	221	215
Nb	86	87	87	76	78	77	90	90	84	73	67	75	60	64
Ba	641	614	622	3474	634	601	737	680	618	607	571	621	537	487
La	75·5	89·0	77·9	74·4	61·0	65·0	72·2	70·5	66·4	56·2	54·1	49·6	60·9	57·9
Ce	141·3	154·6	156·7	137·7	125·2	125·4	144·4	134·7	128·4	109·0	92·2	91·6	118·3	116·9
Nd	59·6	68·4	62·3	52·7	48·5	48·9	55·9	51·7	51·1	45·1	36·9	40·6	46·6	43·2
Sm	11·1	12·9	12·6	11·8	9·50	9·40	11·7	10·6	10·3	8·60	9·00	8·30	9·90	8·30
Eu	3·10	3·36	3·14	3·13	2·50	2·60	2·76	2·75	2·66	2·32	2·03	2·19	2·53	2·55
Gd	9·00	9·25	8·84	9·15	7·86	8·28	7·76	7·74	7·37	7·67	6·61	6·6	7·3	7·20
Dy	6·11	6·51	6·31	6·82	5·34	5·25	6·63	5·84	5·87	5·22	4·57	4·91	5·56	5·58
Er	2·57	2·44	2·51	3·11	2·71	2·90	2·68	2·67	2·66	2·25	2·36	2·13	2·29	2·29
Yb	2·14	2·28	2·11	2·38	2·16	2·27	2·30	2·35	2·14	1·94	1·88	1·87	1·88	1·99
Lu	0·29	0·30	0·29	0·34	0·29	0·30	0·34	0·32	0·28	0·26	0·27	0·28	0·26	0·28

	Bas. HEJ 9	Bas. HEJ 13	Bas. HEJ 14	Bas. HEJ 23	Bas. HEJ 47	Bas. HEJ 48	Bas. HEJ 63a	Bas. HEJ 63b	Bas. HEJ 64	Bas. HEJ 68	Bas. HEJ 44	Bas. HEJ 33
SiO_2	43·86	41·53	41·04	41·60	42·98	42·85	42·22	42·39	41·61	42·67	42·63	43·54
TiO_2	2·01	2·21	2·75	2·25	2·49	2·49	2·46	2·46	2·56	2·35	2·57	2·50
Al_2O_3	13·28	11·16	13·71	12·25	12·17	12·13	13·58	13·60	13·59	12·79	15·05	14·68
Fe_2O_3	3·35	4·20	4·66	3·22	4·93	4·01	4·64	4·47	4·72	4·04	4·18	4·70
FeO	6·89	7·16	7·14	6·84	7·07	7·90	6·26	6·38	6·35	6·52	6·68	5·69
MnO	0·14	0·15	0·15	0·14	0·14	0·14	0·16	0·15	0·16	0·14	0·15	0·15
MgO	10·25	14·39	11·26	13·95	12·47	12·22	11·45	11·54	11·87	14·00	7·99	8·29
CaO	10·60	12·00	12·24	11·81	11·59	11·52	12·01	11·98	12·02	11·34	12·10	12·41

	Bas. HEJ 9	Bas. HEJ 13	Bas. HEJ 14	Bas. HEJ 23	Bas. HEJ 47	Bas. HEJ 48	Bas. HEJ 63a	Bas. HEJ 63b	Bas. HEJ 64	Bas. HEJ 68	Bas. HEJ 44	Bas. HEJ 33
Na_2O	3·03	2·42	2·70	3·02	2·39	2·27	3·11	2·97	2·93	2·73	3·89	3·50
K_2O	1·21	0·68	1·27	0·80	1·23	1·24	1·03	1·10	0·99	0·86	1·45	1·47
P_2O_5	0·42	0·65	0·53	0·40	0·65	0·70	0·57	0·58	0·50	0·44	0·88	0·75
LOI	4·04	2·24	1·97	2·54	1·66	1·94	2·16	2·18	2·19	2·13	2·93	2·36
Total	99·08	98·79	99·42	98·82	99·77	99·41	99·65	99·80	99·49	100·01	100·50	100·04
Mg-no.	66	71	65	73	67	67	67	68	68	72	59	61
Sc	19	20	24	41	16	10	23	17	26	24	27	28
V	225	294	349	292	280	269	313	332	336	306	266	314
Cr	312	712	261	669	440	436	338	335	310	582	143	219
Co	57	67	60	60	58	58	54	49	57	61	41	48
Ni	219	372	157	351	299	287	187	180	214	340	97	115
Cu	63	54	64	73	73	69	77	73	70	88	36	85
Zn	107	84	81	74	95	99	85	90	85	80	87	86
Ga	16	18	18	15	17	15	21	16	16	16	21	22
Rb	37	38	35	29	27	30	40	41	33	37	49	29
Sr	671	656	670	609	726	745	730	716	656	607	1045	1128
Y	22	26	26	25	25	26	25	26	27	25	33	33
Zr	230	192	203	183	214	216	232	233	218	199	265	256
Nb	57	57	76	54	60	65	77	79	68	60	84	82
Ba	483	444	499	443	454	464	610	560	497	498	702	767
La	46·5	41·4	40·8	36·3	41·0	44·2	57·4	54·5	46·5	37·1	69·9	70·2
Ce	85·9	75·0	82·5	66·6	87·5	90·1	120·6	117·2	91·0	76·5	122·2	135·1
Nd	34·0	32·5	34·7	28·1	38·1	42·7	38·8	39·5	38·1	30·5	51·7	50·8
Sm	8·10	7·40	8·50	7·00	8·50	8·80	9·00	9·30	8·90	7·80	10·0	9·20
Eu	1·83	2·07	2·17	1·76	2·62	2·50	2·13	2·12	2·26	2·05	2·81	2·72
Gd	6·31	4·92	6·13	4·71	6·57	6·79	6·24	6·19	6·41	5·37	7·71	7·46
Dy	4·47	4·27	5·19	3·99	4·88	5·46	5·26	5·08	5·52	4·65	5·74	5·62
Er	2·04	1·89	2·38	1·67	2·83	2·40	2·23	2·13	2·48	2·09	2·48	2·55
Yb	1·85	1·44	1·85	1·42	1·69	1·80	1·90	1·85	1·89	1·68	2·01	2·03
Lu	0·24	0·23	0·24	0·18	0·23	0·23	0·28	0·28	0·27	0·25	0·26	0·28

	Bas. HEJ 45	Bas. HEJ 56	Bas. HEJ 57	Bas. HEJ 62	Bas. HEJ 70	Bas. HEJ 21	Bas. HEJ 22	Bas. HEJ 54	Bas. HEJ 55	Bas. HEJ 58	Alk.-Bas. HEJ 71	Alk.-Bas. HEJ 61
SiO_2	43·87	42·70	43·71	44·96	42·12	42·03	41·22	42·34	42·87	44·60	45·24	45·66
TiO_2	2·56	2·66	2·63	2·28	2·50	3·06	3·04	2·35	2·34	2·62	2·34	2·26
Al_2O_3	14·83	14·23	12·84	14·43	13·53	14·29	14·17	11·94	11·94	13·07	14·01	14·01
Fe_2O_3	4·51	4·95	4·16	4·60	5·75	5·00	5·24	3·40	3·74	7·92	5·37	4·06
FeO	6·76	6·63	7·80	5·53	5·42	6·74	6·47	8·67	8·38	4·60	5·73	6·85
MnO	0·14	0·15	0·15	0·14	0·15	0·14	0·13	0·22	0·23	0·13	0·14	0·15
MgO	9·20	8·85	9·48	8·29	9·80	9·83	9·88	9·19	9·88	8·34	9·37	8·95
CaO	10·75	11·11	11·38	10·83	11·86	11·73	11·72	12·75	12·68	11·20	10·64	10·35
Na_2O	3·97	3·76	2·59	2·05	3·09	2·88	2·68	2·56	2·65	2·61	2·42	2·64
K_2O	1·00	1·27	1·25	1·56	0·59	1·00	0·84	1·10	1·10	1·21	1·28	1·73
P_2O_5	0·67	0·75	0·63	0·55	0·71	0·48	0·49	0·57	0·58	0·64	0·53	0·47
LOI	2·34	2·29	1·95	4·25	3·74	1·80	2·82	3·93	3·25	2·32	2·57	2·50
Total	100·60	99·35	98·57	99·47	99·26	98·98	98·70	99·02	99·64	99·26	99·64	99·63

	Bas. HEJ 45	Bas. HEJ 56	Bas. HEJ 57	Bas. HEJ 62	Bas. HEJ 70	Bas. HEJ 21	Bas. HEJ 22	Bas. HEJ 54	Bas. HEJ 55	Bas. HEJ 58	Alk.-Bas. HEJ 71	Alk.-Bas. HEJ 61
Mg-no.	62	60	61	62	64	62	63	60	61	57	63	62
Sc	18	15	17	22	26	31	24	17	18	13	14	17
V	276	270	266	289	273	374	396	244	237	263	247	220
Cr	175	217	319	224	315	182	173	419	409	336	282	271
Co	55	48	47	46	53	61	54	56	52	49	50	49
Ni	131	138	196	109	173	108	107	241	237	196	189	174
Cu	57	66	75	64	74	83	84	79	65	88	66	68
Zn	89	102	99	73	91	83	74	98	92	105	97	103
Ga	22	23	17	13	20	15	19	14	22	21	20	26
Rb	22	62	26	43	25	36	31	25	30	51	40	50
Sr	851	906	721	896	881	697	690	656	640	658	813	890
Y	25	23	28	23	26	28	24	27	21	28	28	28
Zr	229	264	202	212	225	216	211	200	194	198	208	302
Nb	67	89	64	62	84	58	59	51	48	59	72	81
Ba	601	703	514	634	697	492	496	438	429	493	716	861
La	54·5	60·0	46·0	64·4	64·0	44·0	43·1	35·8	31·8	39·9	52·0	52·8
Ce	103·9	121·6	94·5	122·2	114·4	88·1	91·8	83·5	74·0	81·8	91·0	105·5
Nd	43·5	48·3	40·1	41·8	43·9	39·8	38·3	32·5	36·1	33·7	32·2	44·7
Sm	8·2	10·5	9·60	10·3	9·60	8·10	7·70	8·40	7·70	8·00	8·80	9·90
Eu	2·46	2·85	2·65	2·51	2·54	2·32	2·30	2·40	1·92	2·28	2·42	2·25
Gd	6·57	7·14	7·41	6·00	7·13	6·23	6·45	5·82	5·61	6·98	6·25	6·56
Dy	5·27	5·29	6·41	4·92	4·88	5·27	5·16	4·90	4·65	5·38	5·43	4·98
Er	2·26	2·00	2·84	2·05	2·03	2·38	2·57	2·05	2·03	2·06	2·58	2·35
Yb	1·81	1·76	1·98	1·8	1·65	1·89	1·80	1·72	1·33	1·54	1·86	1·72
Lu	0·25	0·25	0·26	0·27	0·23	0·28	0·24	0·24	0·20	0·22	0·28	0·25

	Alk.-Bas. HEJ 53	Alk.-Bas. HEJ 20	Alk.-Bas. HEJ 8	Haw. HEJ 25	Teph. HEJ 1	Haw. HEJ 35	Teph.-Ph. HEJ 37	Mug. HEJ 10	Ben. HEJ 29	Ben. HEJ 11	BB (this study)	BB (rec. val.)	JB 2 (this study)	JB 2 (rec. val.)
SiO_2	45·56	45·32	45·54	47·85	48·21	49·23	53·69	54·61	55·49	56·38	48·81	48·90	53·33	53·20
TiO_2	2·34	2·81	2·51	1·77	1·98	1·86	0·90	1·55	1·43	1·59	2·35	2·33	1·17	1·19
Al_2O_3	13·78	16·39	16·10	16·13	16·93	18·27	19·71	16·68	17·44	18·14	13·67	13·60	14·71	14·67
Fe_2O_3	3·41	6·82	5·45	4·18	4·34	4·25	2·44	2·07	3·65	5·74	11·24	11·20	14·43	14·34
FeO	7·92	4·54	5·34	3·49	4·15	4·56	1·86	4·78	3·23	1·07	n.d.	n.d.	n.d.	n.d.
MnO	0·15	0·14	0·15	0·21	0·15	0·16	0·14	0·17	0·16	0·09	0·18	0·19	0·22	0·20
MgO	8·56	5·16	6·21	5·77	4·25	3·62	1·46	2·25	2·33	0·73	8·54	8·16	4·75	4·66
CaO	10·80	10·07	10·44	8·16	8·24	7·61	4·98	6·07	5·72	4·34	8·51	8·30	9·86	9·89
Na_2O	2·74	2·93	3·54	2·55	4·76	4·91	5·42	4·51	4·71	4·95	3·63	3·97	2·00	2·03
K_2O	1·31	1·48	1·41	2·78	2·63	2·17	4·31	3·00	3·24	3·37	1·77	1·80	0·41	0·42
P_2O_5	0·53	0·67	0·55	0·33	0·42	0·56	0·46	0·58	0·49	0·62	0·52	0·52	0·08	0·10
LOI	2·19	3·25	1·94	6·79	1·98	2·77	5·43	2·33	2·58	1·67	n.d.	n.d.	n.d.	n.a.
Total	99·29	99·58	99·18	100·01	98·04	99·97	100·80	98·60	100·47	98·69	99·22	98·97	100·96	100·70
Mg-no.	60	48	53	60	50	45	40	39	40	18				
Sc	14	8	31	14	14	5	6	3	5	5	8	n.a.	50	54·4
V	232	288	276	210	206	170	77	143	130	142	242	250	595	578
Cr	227	24	104	154	49	5	27	20	38	21	275	250	31	27·4
Co	47	45	51	40	31	31	17	22	19	13	44	45	38	39·8

	Alk.-Bas.	Alk.-Bas.	Alk.-Bas.	Haw.	Teph.	Haw.	Teph.-Ph.	Mug.	Ben.	Ben.	BB (this study)	BB (rec. val.)	JB 2 (this study)	JB 2 (rec. val.)
	HEJ 53	HEJ 20	HEJ 8	HEJ 25	HEJ 1	HEJ 35	HEJ 37	HEJ 10	HEJ 29	HEJ 11				
Ni	164	40	58	77	29	1	14	13	17	12	179	188	12	14·2
Cu	75	32	70	36	21	5	16	10	8	11	40	38	217	227
Zn	99	104	98	88	89	115	96	80	92	129	124	127	108	110
Ga	21	23	17	25	24	25	26	29	29	24	16	24	14	17
Rb	37	24	35	92	67	56	124	107	119	126	48	45	8	6·2
Sr	723	1151	835	638	1137	1330	643	769	741	779	860	849	183	178
Y	25	30	27	19	32	36	22	34	28	30	23	26	23	24·9
Zr	198	269	244	378	334	371	448	410	424	461	226	208	58	51·4
Nb	59	88	65	110	94	112	107	91	88	97	62	65	2	0·8
Ba	537	781	634	1172	1055	1063	975	704	837	743	617	627	207	208
La	47·6	67·3	50·6	66·9	82·5	88·5	76·0	74·8	71·5	84·9	47·2	48·0	n.d.	n.d.
Ce	86·7	122·6	99·8	115·2	155·1	161·5	115·0	150·3	129·1	155·7	91·0	92·0	n.d.	n.d.
Nd	39·2	42·5	37·4	35·9	44·0	55·4	27·9	53·7	54·8	57·0	42·4	43·0	n.d.	n.d.
Sm	10·1	9·60	8·60	7·20	7·80	9·30	4·20	11·0	11·5	10·8	8·10	8·40	n.d.	n.d.
Eu	2·21	2·75	2·19	1·83	2·13	2·65	1·18	2·40	2·34	2·60	2·50	2·50	n.d.	n.d.
Gd	6·97	7·66	7·23	5·11	6·54	7·38	2·91	7·89	7·28	8·55	6·90	6·80	n.d.	n.d.
Dy	5·84	5·58	5·12	4·22	4·88	5·46	2·87	5·82	5·78	5·62	4·50	4·70	n.d.	n.d.
Er	2·58	2·44	2·37	2·49	2·66	2·78	1·64	2·87	2·96	2·95	2·20	2·10	n.d.	n.d.
Yb	1·80	1·95	1·91	2·22	2·43	2·14	2·00	2·80	2·52	2·71	1·80	1·70	n.d.	n.d.
Lu	0·29	0·28	0·25	0·33	0·35	0·30	0·29	0·38	0·35	0·37	0·22	0·23	n.d.	n.d.

Neph., nephelinite; Bas., basanite; Alk.-Bas., alkali basalt; Mug., mugearite; Ben., benmoreite; Haw., hawaiite; Teph., tephrite; Teph. Ph., tephriphonolite; rec. val., recommended values; LOI, loss on ignition; Mg-number = 100 × Mg/[Mg + Fe(tot.)]; n.d., not determined; n.a., not available. JB 2, international rock standard, a tholeiitic basalt from O-shima volcano, Japan (Govindaraju, 1994). BB, in-house standard, a Tertiary alkali olivine basalt from Bramburg (Adelsleben) calibrated against several international rock standards (Engelhardt, 1990).

have high CaO/Al_2O_3 ratios and this ratio decreases in the more differentiated rocks with increasing SiO_2 (Fig. 3b).

Trace element data are reported in Table 3 and Figs 4 and 5. Most nephelinites, basanites and the alkali basalts have Ni, Cr and Co contents that approach the values commonly assumed for primary magmas (e.g. Frey *et al.*, 1978). Scandium contents range from 10 to 40 ppm for the nephelinites, basanites and the alkali basalts (Fig. 4d). The most interesting feature is the strong overlap in compatible trace element abundances for nephelinites, basanites and alkali basalts. Similarly, incompatible trace element abundances (Nb, Ba, Zr, La) show strong overlap in nephelinites, basanites and the alkali basalts (Fig. 5), although the nephelinites tend to have higher La abundances than the basanites and alkali basalts. Consequently, ratios of incompatible trace elements (Zr/Y, La/Nb, Zr/Nb; Fig. 6) also show some overlap for nephelinites, basanites and alkali basalts. On the other hand, ratios of Ba/La, Ba/Nb and K/Nb tend to increase with increasing SiO_2 from nephelinites to basanites and alkali basalts (Fig. 6). Most of the differentiated rocks have higher Ba/La, Ba/Nb, K/Nb, Rb/Nb and Zr/Nb ratios than the nephelinites, basanites and alkali basalts, and Ba/La and Ba/Nb decrease with increasing SiO_2 within this group (Fig. 6). The Rb/Nb and K/Nb ratios are positively correlated and the nephelinites tend to have lower Rb/Nb and K/Nb ratios than the basanites and alkali basalts. The differentiated rocks have the highest Rb/Nb and K/Nb ratios. La/Nb ratios are remarkable constant among the nephelinites, basanites and alkali basalts. Nephelinites, basanites and alkali basalts have light REE (LREE)-enriched REE patterns similar to those of many ocean island basalts (OIB) and alkaline volcanic rocks from continental settings (Fig. 7). The differentiated rocks have similar REE patterns; two samples have a pronounced depletion in middle REE (MREE) (Fig. 7). Nephelinites, basanites and alkali basalts show strong enrichment of highly incompatible and moderately incompatible trace elements (Fig. 8). K and Rb are strongly depleted relative to elements with similar incompatibility (Fig. 8) whereas in some nephelinites, the basanites and alkali basalts additional slight depletions of P and Ti can be observed. Some nephelinites are

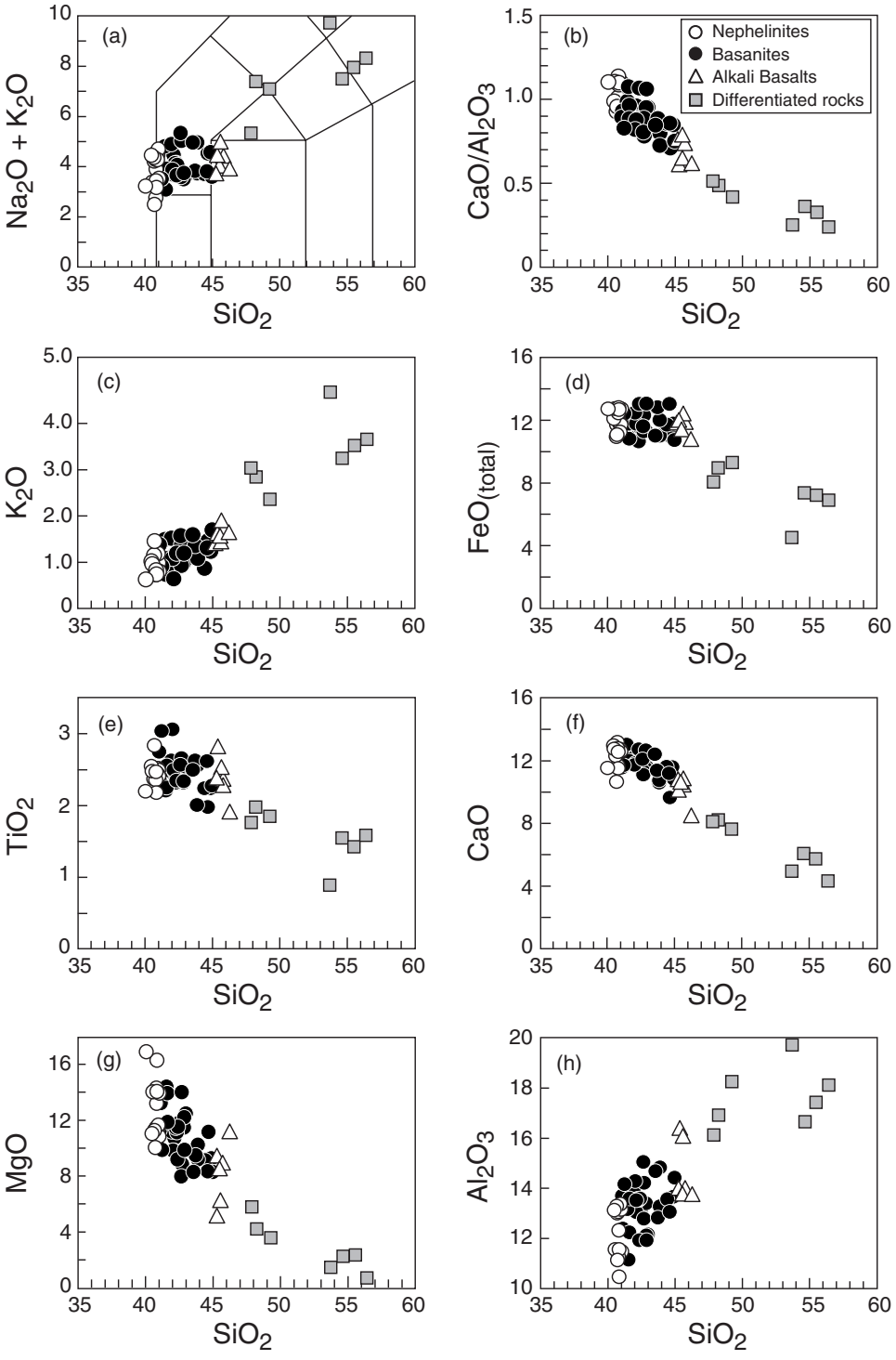

Fig. 3. (a) Total alkali–silica diagram (Le Bas *et al.*, 1986), (b) CaO/Al_2O_3 vs SiO_2, (c) K_2O vs SiO_2, (d) FeO (total) vs SiO_2, (e) TiO_2 vs SiO_2, (f) CaO vs SiO_2, (g) MgO vs SiO_2 and (h) Al_2O_3 vs SiO_2 for the Hocheifel lavas.

enriched in P. Apart from these anomalies, primitive mantle-normalized concentrations increase with increasing incompatibility and show typical OIB or intracontinental basalt patterns (Fig. 8).

Sr–Nd–Pb isotope chemistry

Sr–Nd–Pb isotope data are reported in Table 4. The $^{87}Sr/^{86}Sr$ ratios of the Hocheifel basalts are low and the $^{143}Nd/^{144}Nd$ ratios are high; thus, the samples plot in

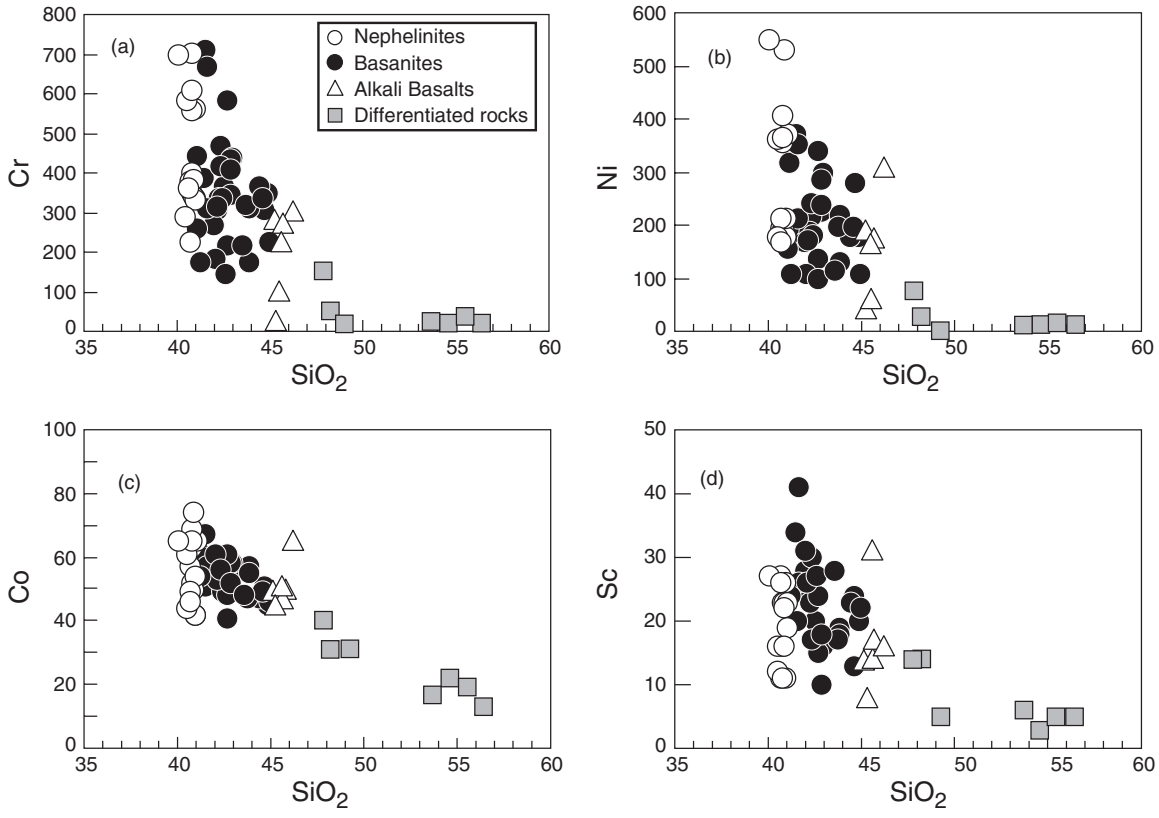

Fig. 4. (a) Cr (in ppm) vs SiO_2 (wt %), (b) Ni (in ppm) vs SiO_2, (c) Co (in ppm) vs SiO_2 and (d) Sc (in ppm) vs SiO_2 for the Hocheifel lavas.

the 'depleted field' relative to Bulk Earth in the Sr–Nd isotope diagram (Fig. 9). Sr and Nd isotope data for the primitive nephelinites, basanites and alkali basalts form an elongated trend from more depleted compositions similar to the European Asthenospheric Reservoir (EAR; Cebriá & Wilson, 1995) towards Bulk Earth values. Generally, this trend is broadly similar to the trends defined by Cenozoic mafic alkaline rocks from elsewhere in Germany (Wörner *et al.* 1986; Wedepohl *et al.*, 1994; Hegner *et al.*, 1995; Jung & Masberg, 1998; Jung & Hoernes, 2000; Bogaard & Wörner 2003; Haase *et al.*, 2004) and also to other CEVP provinces; for example, the Massif Central, Poland, and the Pannonian basin (Alibert *et al.*, 1987; Blusztajn & Hart, 1989; Downes, 1984; Wilson & Downes, 1991, 2006; Embey-Isztin *et al.*, 1993; Harangi, 1994; Downes *et al.*, 1995). It is noteworthy that the trend defined by the Hocheifel lavas is similar to that of the neighbouring East Eifel and West Eifel volcanic fields (Wörner *et al.*, 1985), which is, however, displaced to slightly higher $^{87}Sr/^{86}Sr$ ratios at a given $^{143}Nd/^{144}Nd$ ratio. The more differentiated samples tend to have more radiogenic $^{87}Sr/^{86}Sr$ and less radiogenic $^{143}Nd/^{144}Nd$ than the mafic alkaline lavas and overlap with the compositional fields of Eifel mantle xenoliths and lower crustal granulite xenoliths (Fig. 9).

The Pb isotope compositions of the nephelinites, basanites and alkali basalts overlap and are variable, defining a linear array subparallel to the Northern Hemisphere Reference Line (NHRL). This trend ranges from high $^{206}Pb/^{204}Pb$ ratios (~20) similar to the EAR to more unradiogenic values (~19) similar to other volcanic provinces from the CEVP (Fig. 10). A subset of basanites has distinctly lower $^{207}Pb/^{204}Pb$ ratios than the other samples (Fig. 10). Published Pb isotope data for East Eifel and West Eifel volcanic fields have slightly higher $^{207}Pb/^{204}Pb$ and $^{208}Pb/^{204}Pb$ ratios at a given $^{206}Pb/^{204}Pb$ ratio (Wörner *et al.*, 1986).

DISCUSSION

Fractional crystallization

Most of the nephelinites, basanites and alkali basalts from the Hocheifel volcanic field have MgO, Cr and Ni contents high enough for these rocks to represent near-primary magmas (e.g. Hart & Davies, 1978). Some samples have lower concentrations of MgO, Ni and Cr, and for these samples fractionation of olivine and

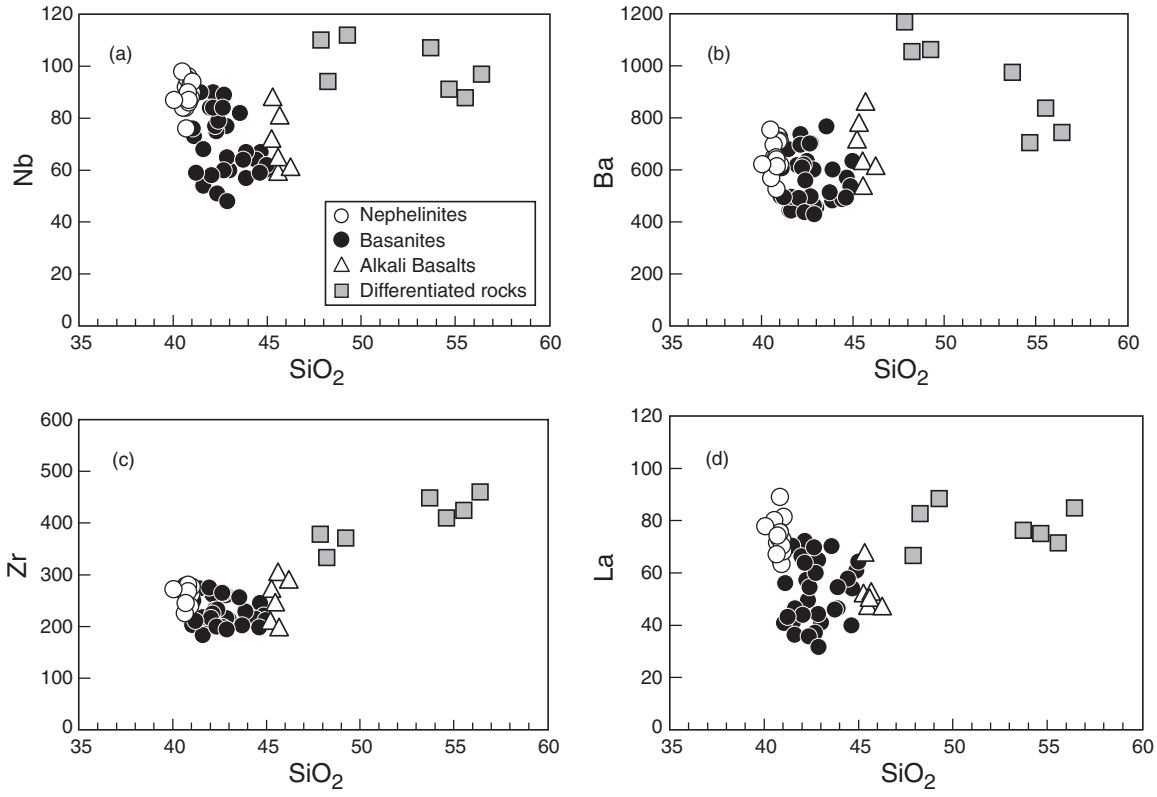

Fig. 5. (a) Nb (in ppm) vs SiO_2 (wt %), (b) Ba (in ppm) vs SiO_2, (c) Zr (in ppm) vs SiO_2 and (d) La (in ppm) vs SiO_2 for the Hocheifel lavas.

clinopyroxene is likely. For these samples, decreasing CaO and increasing Al_2O_3 leds to decreasing CaO/Al_2O_3 ratios with increasing SiO_2, which is also consistent with clinopyroxene fractionation. Increasing Al_2O_3 contents and the lack of negative Eu anomalies indicate that plagioclase was not a major fractionating mineral phase at this stage, implying that fractionation took place at pressures >5 kbar, equivalent to depths >15 km within the lower crust. The more differentiated rocks have the lowest Ni, Cr and V abundances, indicating that olivine, clinopyroxene and Fe–Ti oxides were important fractionating mineral phases in the petrogenesis of the more evolved Hocheifel magmas. In accordance with previous studies on the evolution of alkaline magma series, it is suggested that the alkali basalts represent the parental magmas from which the more differentiated rocks originated by fractional crystallization (Wilson *et al.*, 1995). The three most differentiated samples with SiO_2 > 50 wt % (HEJ 10, HEJ 11, HEJ 29) have the lowest Sr/Nd ratio and small negative Eu anomalies, indicating removal of Sr by plagioclase fractionation (Fig. 7). Another fractionated sample (HEJ 37; Fig. 7) shows a deficency of the MREE relative to the LREE and heavy REE (HREE), which can be explained by significant fractionation of amphibole and/or titanite. Some nephelinites and basanites, and most of the alkali basalts, contain green-core clinopyroxenes; in accordance with previous studies (e.g. Duda & Schmincke, 1985; Jung & Hoernes, 2000; Haase *et al.*, 2004) the appearence of green-core clinopyroxenes (with cores enriched in Al, Fe and Na and with low Ti/Al ratios) is evidence for high-pressure or, at least, polybaric fractionation of the host magmas. Polybaric fractionation at deep crustal levels may also be associated with crustal contamination, which will be evaluated below.

Crustal contamination

Major element and compatible trace element variations in the alkali basalts and the more differentiated rocks of the Hocheifel indicate that fractional crystallization processes affected the magmas during ascent. Fluid-inclusion barometric studies have shown that similar alkaline magmas from the Quaternary Eifel volcanic field stagnated in the lower crust at pressures of about 0·65 GPa, equivalent to 20 km depth (Duda & Schmincke, 1985; Sachs & Hansteen, 2000). In view of the occurrence of petrographically similar, green-core, clinopyroxenes in most of the alkali basalts, basanites and nephelinites (Table 1) from the Hocheifel, it is suggested that these magmas also stagnated in the lower crust at comparable depths.

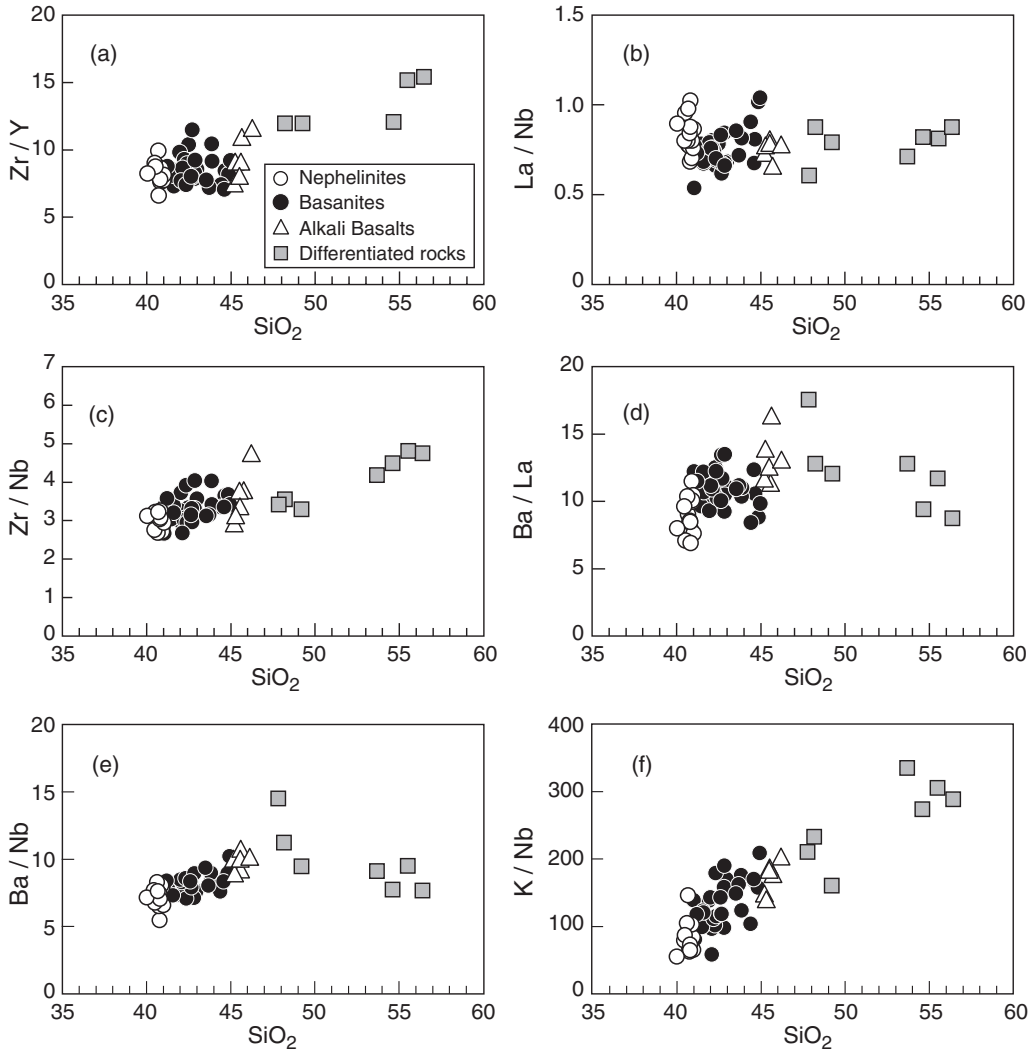

Fig. 6. (a) Zr/Y vs SiO_2, (b) La/Nb vs SiO_2, (c) Zr/Nb vs SiO_2, (d) Ba/La vs SiO_2, (e) Ba/Nb vs SiO_2 and (f) K/Nb vs SiO_2 for the Hocheifel lavas.

The lower crust beneath the Eifel is composed of mafic and felsic granulites, in which mafic granulites, interpreted as basaltic cumulates, predominate over felsic granulites (Mengel *et al.*, 1991; Sachs & Hansteen, 2000). The upper crust consists of Palaeozoic sedimentary and volcanic rocks as well as rare Mesozoic and Cenozoic sedimentary rocks. Rare metasedimentary granulites also occur. Some granulites show evidence of metasomatism and partial melting (formation of secondary hydrous phases, presence of glass) and it has been shown that this metasomatic event is most probably related to the Quaternary–Tertiary magmatism (Sachs & Hansteen, 2000). Lower crustal xenoliths from the Eifel have been extensively studied (Stosch & Lugmair, 1984; Stosch *et al.*, 1986, 1992; Loock *et al.*, 1990; Rudnick & Goldstein, 1990) and, therefore, major and trace element and Sr–Nd–Pb isotope data are available. These granulites have Sr–Nd isotope compositions that extend from Bulk Earth values towards more unradiogenic $^{143}Nd/^{144}Nd$ but more radiogenic $^{87}Sr/^{86}Sr$ isotope compositions (Fig. 9). Felsic granulites tend to have more radiogenic $^{87}Sr/^{86}Sr$ isotope compositions, although some mafic granulites are also fairly radiogenic. The nephelinites, basanites and alkali basalts have higher $^{143}Nd/^{144}Nd$ and lower $^{87}Sr/^{86}Sr$ than the lower crustal xenoliths, and only a few of the more differentiated rocks overlap with the Sr–Nd isotope composition of the xenoliths (Fig. 9). The Pb isotope compositions of the xenoliths plot above the NHRL in $^{207}Pb/^{204}Pb$ vs $^{206}Pb/^{204}Pb$ and $^{208}Pb/^{204}Pb$ vs $^{206}Pb/^{204}Pb$ space (Fig. 10). Metasedimentary granulitic xenoliths have higher $^{87}Sr/^{86}Sr$ and lower $^{143}Nd/^{144}Nd$ than the mafic and felsic granulites, but similar Pb isotope compositions to them.

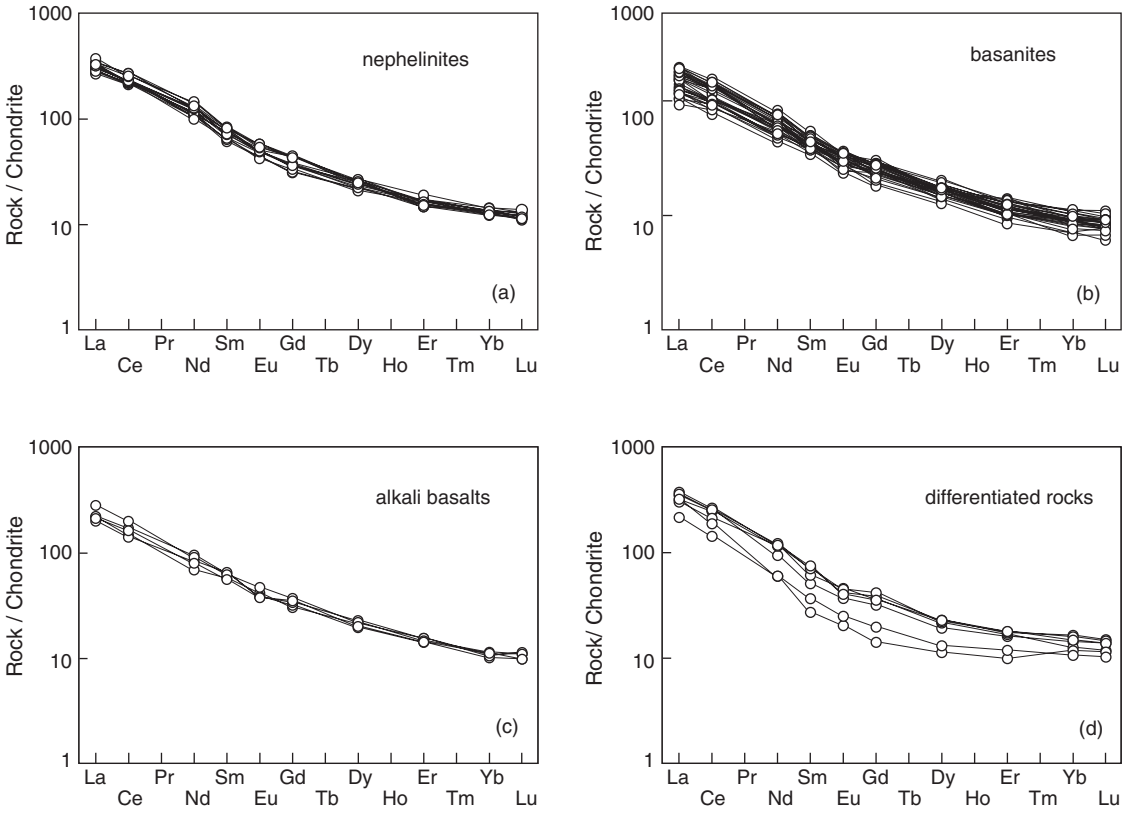

Fig. 7. Rare earth element abundances of (a) nephelinites, (b) basanites, (c) alkali basalts and (d) more differentiated rocks from the Hocheifel area. Normalization values are from Boynton (1984).

The primitive nephelinites, basanites and alkali basalts have a considerable spread in K/Nb that ranges from 52 to 209 despite their limited variation in SiO_2 (Fig. 6). For the CEVP as a whole the range in K/Nb ratios has been explained as a result of mixing of partial melts of two different mantle end-members (Wilson & Downes, 1991). On the other hand, the positive correlation between K/Nb and SiO_2 (Fig. 6), and the highest K/Nb ratios in the most evolved samples may also reflect crustal contamination processes, as all crustal components (lower crust, bulk crust, upper crust) have high K/Nb ratios (>500; Taylor & McLennan, 1985).

Primitive alkaline volcanic rocks with OIB affinities commonly have low Zr/Nb ratios ranging from ~2 to ~4 (Weaver, 1991), whereas the continental crust has higher and more variable Zr/Nb ratios ranging from ~8 to ~14 (Taylor & McLennan, 1985; Rudnick & Fountain, 1995). The higher Zr/Nb ratios in most of the differentiated lavas and the observed correlations of Zr/Nb and Zr, Zr/Nb and K/Nb, Zr/Nb and $^{87}Sr/^{86}Sr$, and Zr/Nb and $^{143}Nd/^{144}Nd$ suggest assimilation of lower crustal rocks with a composition similar to that of lower crustal xenoliths from the Eifel (Fig. 11). Assimilation of lower crustal rocks and fractional crystallization would have occurred simultaneously. However, thermal considerations suggest that bulk assimilation of lower crustal rocks is unlikely and that contamination of the fractionating alkali mafic magma with a partial melt of the lower crustal wall-rocks is more appropriate. The heat required for partial melting is released by the fractional crystallization process. Recent models indicate that this process is an energy-constrained assimilation–fractional crystallization process (EC-AFC; Spera & Bohrson, 2001). The Spera & Bohrson (2001) model was used to test the influence of concurrent crustal assimilation and fractional crystallization upon the composition of the differentiated lavas from the Hocheifel using the parameters given in Table 4. In contrast to the model parameters given by Spera & Bohrson (2001), we used a higher initial temperature for the lower crust of 900°C. This higher temperature is in agreement with recent estimates of lower crustal temperatures from the Eifel (>800°C, Sachs & Hansteen, 2000), and probably mirrors more closely the effects of rifting, uplift of the asthenosphere–lithosphere boundary and continuing magmatism in Tertiary–Quaternary times. Moreover, at this high inferred temperature, high rates of assimilation relative to fractional crystallization are likely (Reiners

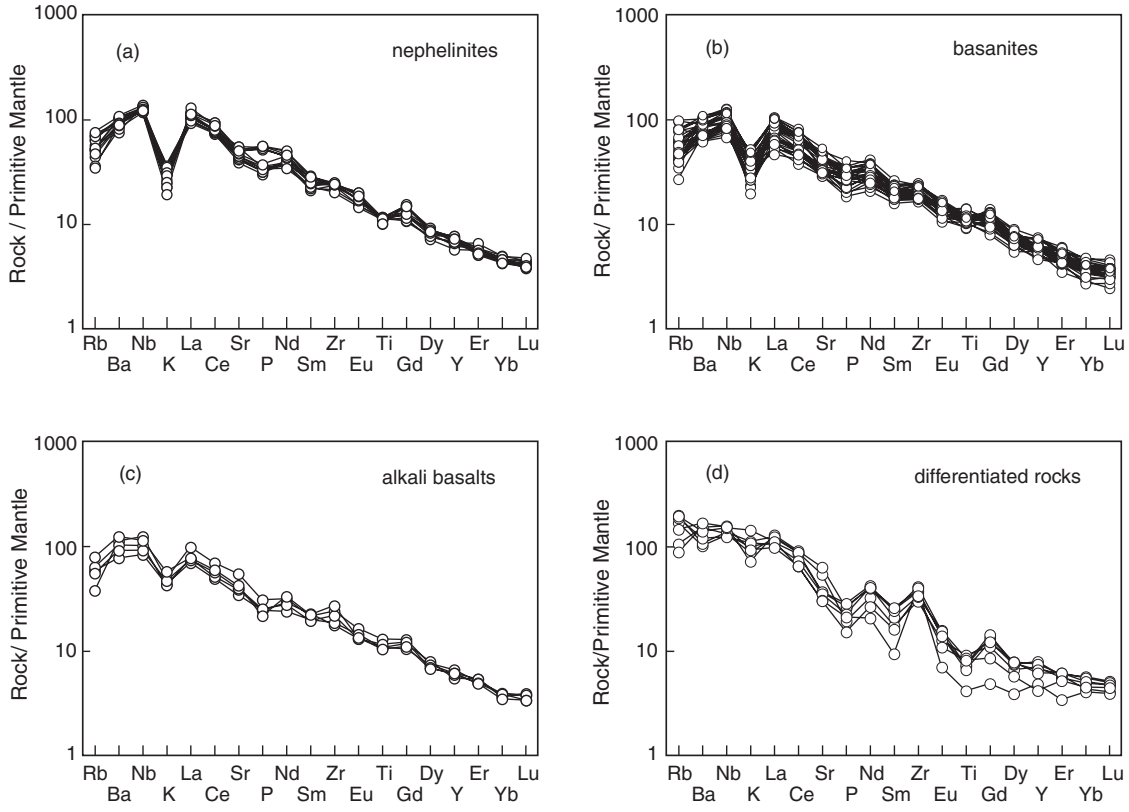

Fig. 8. Primitive mantle-normalized incompatible element patterns of (a) nephelinites, (b) basanites, (c) alkali basalts and (d) more differentiated rocks from the Hocheifel area. Normalization values are from Sun & McDonough (1989).

et al., 1995). In our model, we used sample HEJ 53 as the parental melt; this is one of the most unfractionated alkali basalts based on its moderately high Ni and Cr abundances and low $^{87}Sr/^{86}Sr$ and high $^{143}Nd/^{144}Nd$ isotope ratios (Tables 2 and 3). As the assimilant we used sample S 32 (Stosch & Lugmair, 1984; Loock *et al.*, 1990), which is a mafic granulite xenolith with fairly high $^{87}Sr/^{86}Sr$ and low $^{143}Nd/^{144}Nd$. Zr and Nb concentrations are not available for this granulite xenolith and for modelling purposes we used 70 ppm Zr and 6 ppm Nb (average of lower crust; Taylor & McLennan, 1985) for our lower crustal contaminant. It can be seen that the range in Sr and Nd isotope composition, Zr/Nb and K/Nb ratios and Zr concentrations of the differentiated lavas can be reproduced by an EC-AFC model (Fig. 11), implying that energy-constrained assimilation–fractional crystallization processes played an important role in the evolution of the differentiated lavas from the Hocheifel. Based on this model, the trace element and isotope composition of some of the differentiated lavas can be explained by 40–70% fractional crystallization and 10–50% assimilation of a granulite-facies lower crust with a trace element and isotope composition similar to S 32 (Figs 11 and 12). The degrees of assimilation are rather high and probably unrealistic; however, the composition of the lower crust beneath the Rhenish Massif is somewhat unconstrained with respect to its trace element and isotope composition and more suitable end-members may exist.

Magma generation and partial melting processes

It is generally accepted that the upper mantle is composed predominantly of peridotite with minor amounts of pyroxenite, both with or without garnet. Primitive alkaline, silica-undersaturated melts such as nephelinites and basanites can form at high pressure from garnet peridotite sources (Kushiro, 1996), but not from garnet pyroxenite (Rapp *et al.*, 1991). Therefore, the most likely magma source for the primitive nephelinites and basanites from the Hocheifel is a garnet peridotite. The strong fractionation of HREE, with Dy/Yb >2 (Fig. 13), further suggests that the primitive lavas from the Hocheifel represent partial melts of garnet peridotite. Seismic models indicate that the lithosphere–asthenosphere boundary beneath the Rhenish Massif is strongly elevated and is located at ~50–60 km (Babuska & Plomerová, 1992; Goes *et al.*, 2000), whereas the transition from garnet to

Table 4: Sr, Nd, and Pb isotope compositions of Hocheifel lavas

Sample	Rock type	$^{87}Sr/^{86}$ Sr(m)	$^{87}Sr/^{86}$ Sr(i)	$^{143}Nd/^{144}$ Nd(m)	$^{143}Nd/^{144}$ Nd(i)	$^{206}Pb/^{204}$ Pb(m)	$^{207}Pb/^{204}$ Pb(m)	$^{208}Pb/^{204}$ Pb(m)	$^{206}Pb/^{204}$ Pb(i)	$^{207}Pb/^{204}$ Pb(i)	$^{208}Pb/^{204}$ Pb(i)
HEJ 5	Neph.	0·703260(11)	0·703189	0·512934(08)	0·512897	19·79	15·61	39·59	19·59	15·60	39·32
HEJ 18	Neph.	0·703290(12)	0·703208	0·512933(10)	0·512900	19·79	15·61	39·62	19·59	15·60	39·35
HEJ 50	Neph.	0·703352(12)	0·703292	0·512960(12)	0·512929	19·70	15·60	39·48	19·50	15·59	39·21
HEJ 59	Neph.	0·703279(11)	0·703223	0·512911(09)	0·512880	19·62	15·60	39·43	19·42	15·59	39·17
HEJ 67	Neph.	0·703286(10)	0·703209	0·512949(07)	0·512919	19·70	15·62	39·58	19·50	15·62	39·31
HEJ 26	Neph.	0·703452(12)	0·703411	0·512827(06)	0·512796	19·47	15·58	39·21	19·27	15·57	38·95
HEJ 27	Neph.	0·703423(17)	0·703379	0·512871(14)	0·512837	20·17	15·65	39·94	19·97	15·64	39·67
HEJ 28	Neph.	0·703454(18)	0·703419	0·512876(12)	0·512843	20·01	15·61	39·71	19·81	15·60	39·44
HEJ 30	Neph.	0·703443(10)	0·703409	0·512888(09)	0·512857	19·48	15·60	39·25	19·28	15·59	38·99
HEJ 31	Neph.	0·703554(09)	0·703500	0·512820(11)	0·512789	19·43	15·60	39·24	19·23	15·59	38·98
HEJ 32	Neph.	0·703473(20)	0·703428	0·512878(13)	0·512845	19·79	15·61	39·57	19·59	15·60	39·30
HEJ 24	Neph.	0·703319(14)	0·703271	0·512895(10)	0·512858	19·62	15·57	39·25	19·42	15·56	38·99
HEJ 2	Bas.	0·703341(08)	0·703275	0·512906(10)	0·512874	19·39	15·58	39·19	19·19	15·57	38·93
HEJ 34	Bas.	0·703307(12)	0·703213	0·512960(07)	0·512926	19·48	15·64	39·39	19·28	15·63	39·13
HEJ 46	Bas.	0·703287(09)	0·703222	0·512891(09)	0·512858	19·61	15·59	39·40	19·41	15·58	39·13
HEJ 4	Bas.	0·703337(11)	0·703260	0·512927(07)	0·512896	19·47	15·63	39·44	19·27	15·62	39·17
HEJ 7	Bas.	0·703308(12)	0·703176	0·512917(10)	0·512883	19·48	15·58	39·25	19·28	15·57	38·98
HEJ 9	Bas.	0·703533(19)	0·703445	0·512901(10)	0·512862	19·47	15·64	39·33	19·27	15·63	39·06
HEJ 13	Bas.	0·703378(09)	0·703285	0·512886(12)	0·512848	19·27	15·57	39·10	19·06	15·56	38·83
HEJ 14	Bas.	0·703143(08)	0·703059	0·512947(09)	0·512906	19·70	15·61	39·48	19·50	15·60	39·21
HEJ 23	Bas.	0·703273(10)	0·703197	0·512927(08)	0·512886	19·47	15·59	39·25	19·27	15·58	38·99
HEJ 47	Bas.	0·703474(28)	0·703414	0·512916(08)	0·512879	19·37	15·59	39·17	19·17	15·58	38·90
HEJ 63a	Bas.	0·703446(13)	0·703358	0·512901(10)	0·512863	19·72	15·60	39·45	19·52	15·59	39·18
HEJ 68	Bas.	0·703299(12)	0·703201	0·512921(08)	0·512879	19·72	15·59	39·42	19·51	15·58	39·16
HEJ 16	Bas.	0·703399(10)	0·703350	0·512868(11)	0·512833	19·22	15·50	38·66	19·02	15·49	38·40
HEJ 45	Bas.	0·703212(29)	0·703171	0·512964(15)	0·512933	19·30	15·46	38·81	19·10	15·45	38·54
HEJ 57	Bas.	0·703587(08)	0·703529	0·512781(09)	0·512742	19·19	15·46	38·71	18·99	15·45	38·45
HEJ 70	Bas.	0·703251(10)	0·703205	0·512825(09)	0·512789	n.d.	n.d.	n.d.	n.d.	n.d.	n.d.
HEJ 21	Bas.	0·703446(14)	0·703363	0·512775(08)	0·512741	19·88	15·61	39·61	19·68	15·60	39·38
HEJ 54	Bas.	0·703289(08)	0·703228	0·512843(09)	0·512800	19·13	15·48	38·65	18·93	15·47	38·39
HEJ 58	Bas.	0·703312(07)	0·703188	0·512790(06)	0·512751	19·17	15·50	38·75	18·97	15·49	38·49
HEJ 44	Bas.	0·703236(12)	0·703161	0·512834(08)	0·512802	19·89	15·64	39·69	19·69	15·63	39·42
HEJ 61	Alk.-Bas.	0·703597(12)	0·703507	0·512790(08)	0·512754	19·21	15·53	38·82	19·01	15·53	38·56
HEJ 53	Alk.-Bas.	0·703339(11)	0·703257	0·512840(08)	0·512798	19·53	15·58	39·18	19·33	15·57	38·91
HEJ 20	Alk.-Bas.	0·703315(10)	0·703282	0·512792(09)	0·512755	19·13	15·28	37·94	18·94	15·27	37·68
HEJ 8	Alk.-Bas.	0·703283(14)	0·703216	0·512826(06)	0·512788	19·81	15·60	39·48	19·60	15·59	39·21
HEJ 1	Teph.	0·703541(13)	0·703446	0·512862(15)	0·512833	19·83	15·64	39·68	19·62	15·63	39·41
HEJ 35	Haw.	0·703408(18)	0·703340	0·512851(12)	0·512823	19·26	15·63	39·40	19·06	15·62	39·13
HEJ 10	Mug.	0·704464(13)	0·704241	0·512693(09)	0·512659	19·17	15·50	38·71	18·97	15·49	38·45
HEJ 11	Ben.	0·704538(16)	0·704279	0·512727(14)	0·512696	19·40	15·62	39·26	19·23	15·60	39·00
HEJ 29	Ben.	0·704785(14)	0·704527	0·512606(15)	0·512571	19·29	15·67	39·12	19·09	15·67	38·86
HEJ 37	Teph.-Ph.	0·703669(17)	0·703360	0·512820(15)	0·512795	19·80	15·60	39·44	19·59	15·59	39·17
HEJ 25	Haw.	0·703474(15)	0·703243	0·512905(22)	0·512872	19·82	15·58	39·42	19·61	15·57	39·15

Numbers in parentheses are 2σ in-run deviations of the measurements. Initial Sr and Nd isotope composition were recalculated using Rb, Sr, Sm and Nd concentrations from Table 2 and an age of 40 Ma. Pb isotopic compositions were recalculated using U/Pb = 0·5 and Th/U = 3·5. m, measured; i, initial; n.d., not determined.

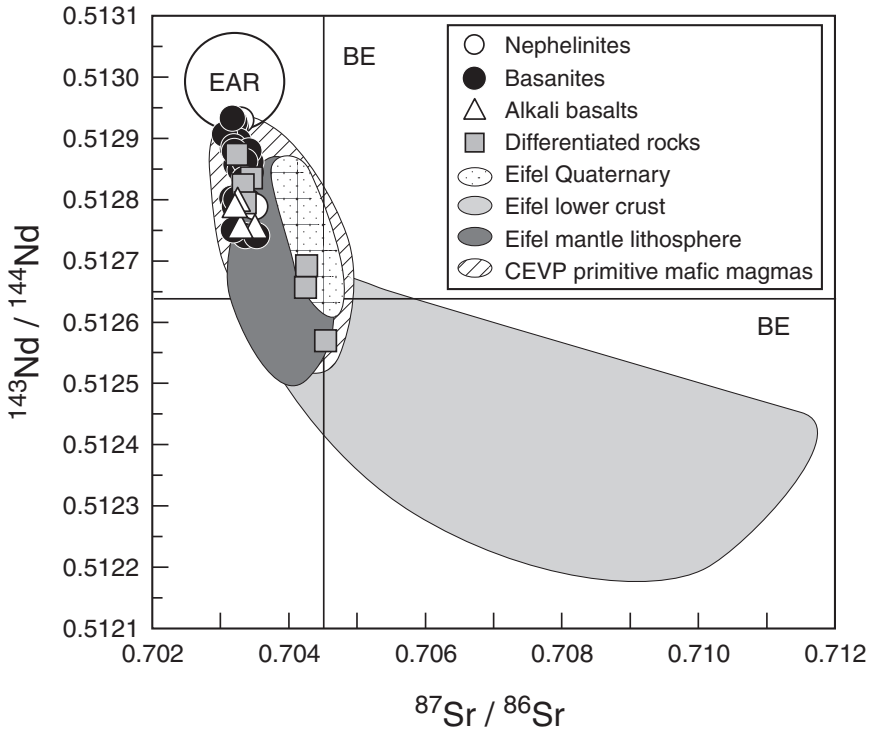

Fig. 9. $^{143}Nd/^{144}Nd$ vs $^{87}Sr/^{86}Sr$ for the Hocheifel mafic alkaline lavas and more differentiated rocks. Stippled area represents data for the Quaternary Eifel volcanic field (Wörner *et al.*, 1986). Dark grey area represents Eifel peridotite xenolith data from Stosch & Lugmair (1986) and Witt-Eickschen *et al.* (1998, 2003). Light grey field represents Eifel lower crustal xenolith data (Stosch &Lugmair, 1984; Loock *et al.*, 1990). EAR, European Asthenospheric Reservoir (Cebriá & Wilson, 1995).

spinel peridotite is estimated at 2·5–3·0 GPa, equivalent to 75–90 km depth (McKenzie & Bickle, 1988; Robinson & Wood, 1998). Previous xenolith-based studies on the composition of the upper mantle beneath the Rhenish Massif indicate that the upper mantle consists of metasomatized spinel peridotite with amphibole and phlogopite (Witt-Eickschen & Kramm, 1998; Witt-Eickschen *et al.*, 1998, 2003).These xenoliths are interpreted to represent fragments of the lithospheric mantle, and it is reasonable to assume that partial melting must have occurred at depths in excess of 60 km (i.e. below the base of the lithosphere).

A useful approach to model partial melting of common upper mantle sources is based on REE systematics (e.g. a plot of La/Yb vs Dy/Yb, Fig. 13; Thirlwall *et al.*, 1994; Baker *et al.*, 1997); such plots can easily distinguish between melting in the garnet peridotite stability field and melting in the spinel peridotite stability field because of the strong fractionation of HREE by garnet. Additionally, mixing of melts from garnet and spinel peridotite sources should produce linear arrays in such a diagram. The nephelinites and most basanites and alkali basalts appear to form a coherent group with higher La/Yb ratios than the rest of the basanites and one alkali basalt, which form another group with higher Dy/Yb ratios (Fig. 13). Considering each group individually, it appears that the samples plot on mixing lines between melts from garnet peridotite and melts from spinel peridotite. Moreover, this diagram suggests that simple partial melting exclusively in the garnet peridotite stability field or spinel peridotite stability field cannot account for the spread of data. Partial melting of spinel peridotite should also produce a positive correlation between Ce/Yb and Yb abundances. Nephelinites, basanites and alkali basalts appear to show a series of negative correlations between Ce/Yb and Yb abundances (Fig. 14a). Additionally, nephelinites, basanites and alkali basalts show a positive correlation between Ce/Yb and Ce abundance (Fig. 14b). These features indicate that: (1) nephelinites, basanites and alkali basalts originate from sources with similar LREE enrichment; (2) nephelinites represent smaller melt fractions than most basanites and alkali basalts; (3) at least the nephelinites originate from a garnet-bearing source in which, during partial melting, garnet was progressively eliminated from the source. High CaO/Al_2O_3 ratios in the nephelinites and decreasing CaO/Al_2O_3 with increasing SiO_2 in the sequence nephelinite–basanite–alkali basalt are also consistent with increasing degrees of partial melting of a garnet-bearing source. Therefore, the most plausible model that can account for the REE variation involves initial partial melting in the garnet stability field, followed by mixing of melts from garnet

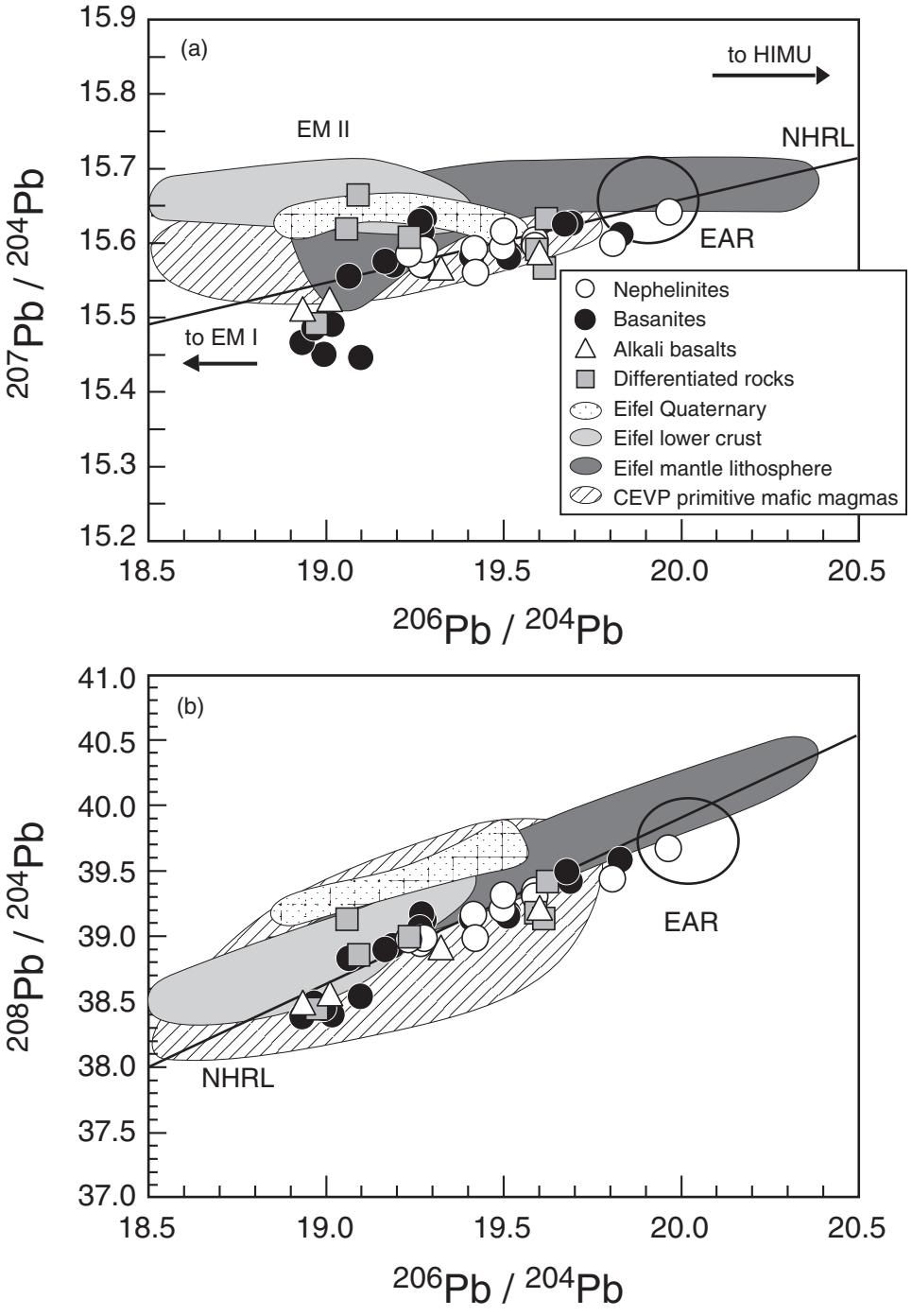

Fig. 10. (a) $^{207}Pb/^{204}Pb$ and (b) $^{208}Pb/^{204}Pb$ vs $^{206}Pb/^{204}Pb$ for Hocheifel mafic alkaline lavas. NHRL, Northern Hemisphere Reference Line (Hart, 1984). Locations of HIMU, EM I and EM II are from Zindler & Hart (1986). Other fields are as in Fig. 8.

peridotite with melts from spinel peridotite, both containing amphibole. Most of these samples cluster at Dy/Yb ratios between 2 and 3; this is typical for the upper mantle beneath the CEVP; the mantle xenoliths have flat to slightly LREE-enriched REE patterns (Stosch & Lugmair, 1986; Witt-Eickschen & Kramm, 1998).

It is noteworthy that the nephelinites, basanites and alkali basalts have a large range in K/La ratios and that the nephelinites have the highest $Ce/Yb_{(norm.)}$ and La concentrations and the lowest K/La ratios (Fig. 15). The model curves shown in Fig. 15 imply that the primitive Hocheifel lavas could result from 1–2% partial

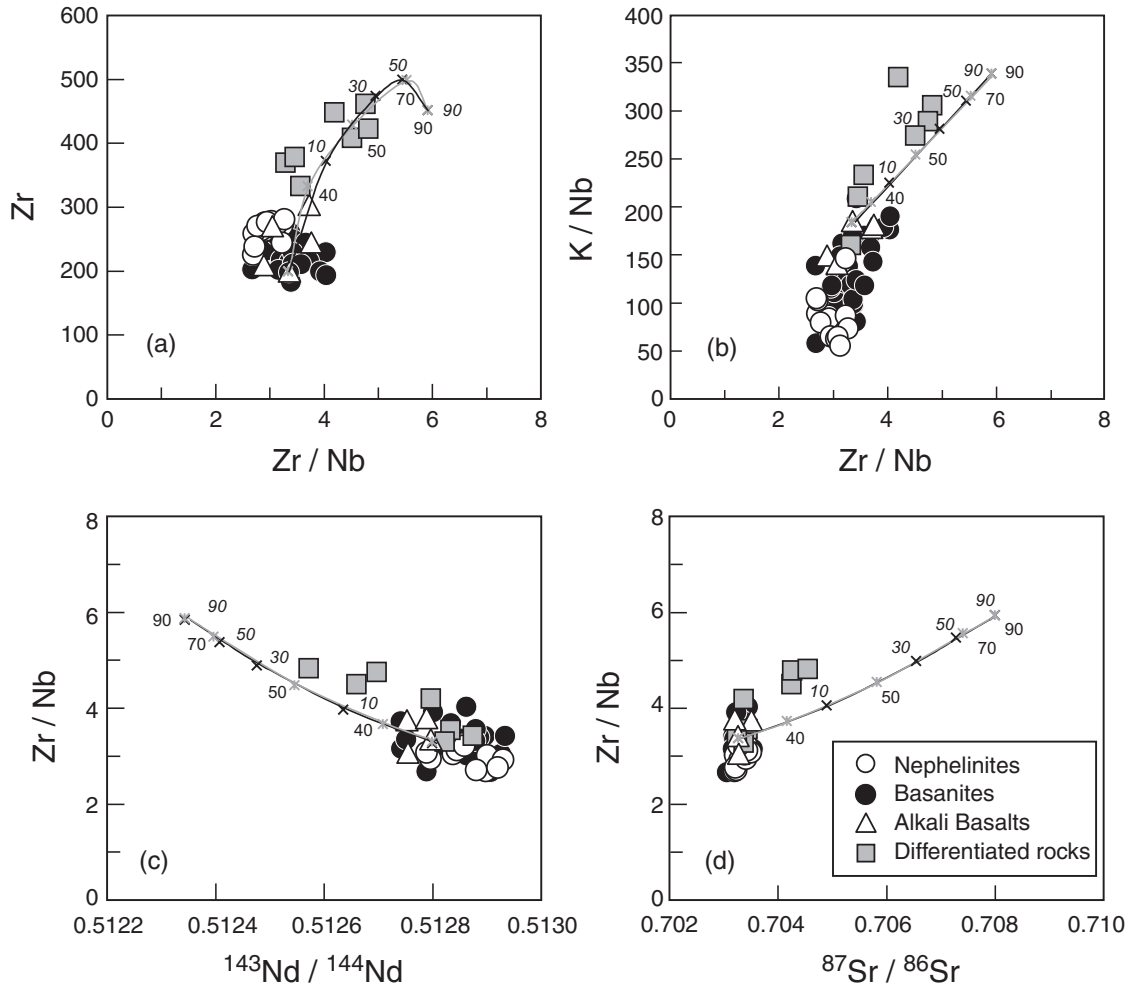

Fig. 11. (a) Zr/Nb vs Zr, (b) Zr/Nb vs K/Nb, (c) Zr/Nb vs ^{143}Nd/^{144}Nd and (d) Zr/Nb vs ^{87}Sr/^{86}Sr for mafic alkaline lavas from the Hocheifel. Lines show the results of EC-AFC calculations with model parameters and end-member compositions from Table 4. Grey lines with regular-font numbers denote mass crystallized and black lines with italic numbers denote mass assimilated, both as wt %.

melting in the garnet peridotite stability field, compatible with experimental results that indicate melting degrees in excess of 1% to generate basanites from peridotite sources (Kushiro, 1996). Similar low degrees of melting have been inferred from a number of volcanic provinces of the CEVP (Wilson & Downes, 2006). In the Hocheifel, small-degree partial melts from garnet-bearing peridotite were mixed with melts produced by a similar degree of melting of a spinel peridotite source (Fig. 13), suggesting that partial melting and mixing of melts occurred close to the spinel–garnet transition zone. The transition from garnet peridotite to spinel peridotite occurs at 2·5–2·7 GPa (Robinson & Wood, 1998), indicating that the Hocheifel lavas formed at ~80 km depth. The nephelinites, basanites and alkali basalts display a negative correlation between K/La and $Ce/Yb_{(norm.)}$ (Fig. 15a) implying that partial melting of garnet or spinel peridotite alone is not likely because low-melt fractions from such sources have both high $Ce/Yb_{(norm.)}$ and K/La ratios (Haase *et al.*, 2004). It is, therefore, very likely that a residual mineral phase that fractionates K from La was present. This mineral phase was probably amphibole rather than phlogopite, because phlogopite fractionates K/La even more efficiently than amphibole and also fractionates Ba/La. Additionally, Ba concentrations are high in the primitive Hocheifel lavas, which argues against significant amounts of phlogopite in the melt residue. Because the nephelinites with high $Ce/Yb_{(norm.)}$ and low K/La ratios formed in the stability field of garnet peridotite in the presence of amphibole, it is suggested that the melting region is located at 2·5–3·0 GPa and 1250–1300°C (Fig. 16). The amphibole may have formed by mantle metasomatism caused by migration of small-degree melts from an upwelling plume beneath the Rhenish Massif.

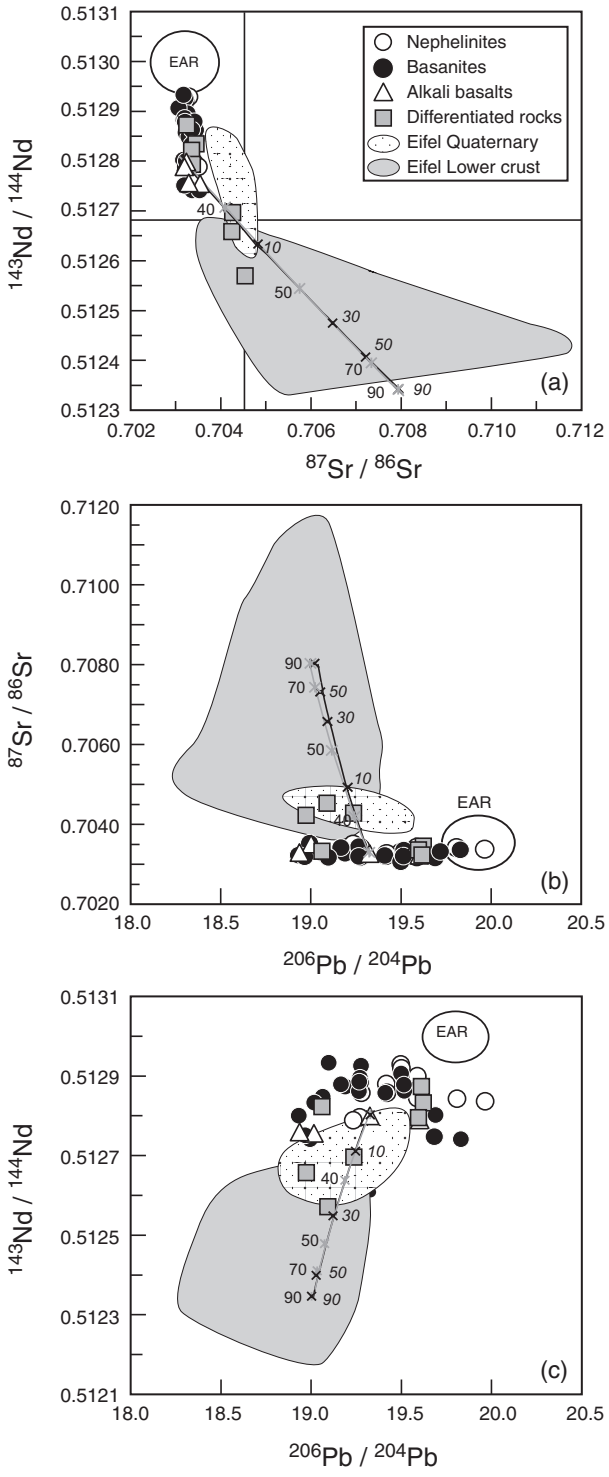

Fig. 12. (a) $^{87}Sr/^{86}Sr$ vs $^{143}Nd/^{144}Nd$, (b) $^{87}Sr/^{86}Sr$ vs $^{206}Pb/^{204}Pb$ and (c) $^{143}Nd/^{144}Nd$ vs $^{206}Pb/^{204}Pb$ for mafic alkaline lavas from the Hocheifel. Lines show the results of EC-AFC calculations with model parameters and end-member compositions from Table 4. Grey lines with regular-font numbers denote mass crystallized and black lines with italic numbers denote mass assimilated both as wt %.

It is still a controversial issue whether the volcanism of the CEVP is related to adiabatic decompression melting caused by thinning of the lithosphere during rifting or due to raised mantle temperatures (up to 200°C, Ritter *et al.*, 2001) as a consequence of mantle plume activity. Data from experimental investigations can be used to constrain the conditions of formation of the Hocheifel lavas. Basanites, and even more Si-undersaturated melts such as nephelinites, can be generated by melting of amphibole- and/or phlogopite-bearing garnet or spinel peridotite at pressures >2 GPa and temperatures >1360°C in the presence of CO_2 (Mysen & Kushiro, 1977; Hirose, 1997). However, similar experimental investigations have shown that the generation of basanites and nephelinites is also possible at much lower temperatures of 1200–1250°C and pressures of 2·8–3·0 GPa (Mengel & Green, 1986; Thibault *et al.*, 1992). The formation of Si-undersaturated melts requires the presence of H_2O and CO_2 (Brey & Green, 1977; Mengel & Green, 1986; Thibault *et al.*, 1992; Hirose, 1997). Magmas with slightly higher SiO_2 concentrations of ~45 wt %, similar to the alkali basalts from the Hocheifel, can be generated from melting of dry mantle at 3·0 GPa (Jaques & Green, 1980; Kushiro, 1996). Results from experimental investigations (Fig. 16) and the REE modelling (Fig. 13) suggest that the primitive Hocheifel lavas (nephelinites, basanites) were generated by melting of garnet peridotite at a pressure of >2·6 GPa at a mantle potential temperature of ~1200°C, which is lower than the inferred average mantle temperature of 1300°C (McKenzie & Bickle, 1988). Huckenholz & Gilbert (1984) and Huckenholz *et al.* (1988) investigated experimentally the stability of Ca-amphibole in a basanite from Alte Burg near Reiferscheid and a nephelinite from the Nürburg. In their experiments, Ca-amphibole was stable between 0·2 GPa/1090°C and 3·0 GPa/1260°C in the basanite and 0·2 GPa/1085°C and 3·0 GPa/1240°C in the nephelinite. Based on these results, Huckenholz & Gilbert (1984) concluded that Ca-amphibole similar in composition to the amphibole that occurs in the mafic alkaline lavas crystallized between 1225°C and 1250°C at pressures of 1·5–2·0 GPa. Assuming that garnet is an important residual phase in the mantle source of the mafic alkaline lavas from the Hocheifel, temperatures of 1250–1300°C at a pressure of 2·5 GPa seems a more reliable *P–T* estimate. The inferred presence of amphibole in the source of the Hocheifel magmas may, therefore, point to a relatively low mantle potential temperature of about 1200–1250°C. Consequently, the data do not support the idea of a very hot mantle source with a maximum excess temperature of 200°C (i.e. Ritter *et al.*, 2001), in the formation of the Hocheifel magmas. This conclusion is also compatible with the view that partial melting in the upper mantle beneath Europe requires

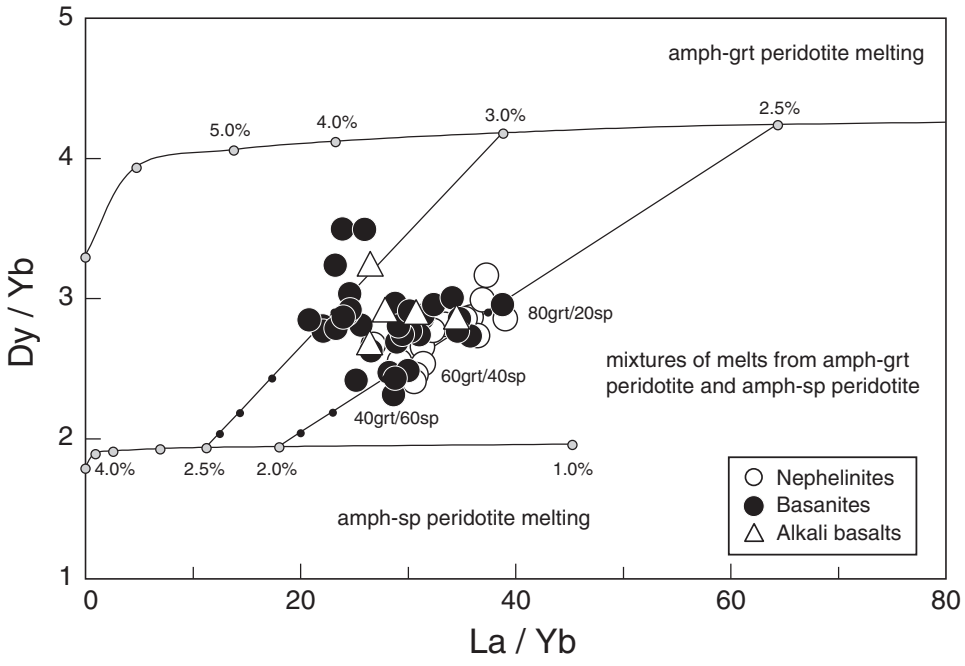

Fig. 13. La/Yb vs Dy/Yb covariation for the Hocheifel basalts. Partial melting curves were calculated using a non-modal, fractional melting model (Shaw, 1970). Sources are grt–amph peridotite (cpx 0·07, opx 0·19, ol 0·55, grt 0·08, amph 0·11), which melts in the proportions cpx 0·25, opx 0·15, ol 0·05, grt 0·3, amph 0·25, and sp–amph peridotite (cpx 0·08, opx 0·25, ol 0·554, sp 0·033, amph 0·083), which melts in the proportions cpx 0·27, opx 0·25, ol 0·08, sp 0·13, amph 0·27. Source composition (La 2·1 ppm, Yb 0·17 ppm, Dy 0·31 ppm) represents average of 36 peridotite xenoliths from the Hessian Depression (Hartmann & Wedepohl, 1990). Mineral–melt distribution coefficients are taken from McKenzie & O'Nions (1991), Hart & Dunn (1993), Kelemen *et al.* (1993), Johnston (1994) and LaTourette *et al.* (1995). Numbers on model curves indicate the per cent melting. Points at 80grt/20sp, 60grt/40sp and 40grt/60sp indicate mixing proportions of melts from garnet peridotite (i.e. 80%) with melts from spinel peridotite (i.e. 20%).

either an anomalously hot mantle (for which we see no evidence here) or a volatile-rich mantle source (Wilson & Downes, 2006) which may be represented by the inferred amphibole-bearing peridotite source of the mafic Hocheifel lavas.

Nature of the mantle sources for the Tertiary Hocheifel basalts

The nephelinites and most basanites and alkali basalts do not appear to have been contaminated by crustal material; hence, their Sr–Nd–Pb isotope compositions should reflect those of their mantle sources. The Sr–Nd–Pb isotope compositions of the primitive Hocheifel lavas exhibit a large range of variation, implying substantial isotopic heterogeneity of the mantle sources involved. The $^{206}Pb/^{204}Pb$ isotope ratios display a large variation ranging from ~19 to ~20, probably indicating mixing of melts from two sources. The Pb isotope values are the highest found to date in the volcanic fields of the Rhenish Massif and exceed the radiogenic Pb isotope compositions of the mafic lavas from the Urach–Hegau volcanic field (Hegner *et al.*, 1995; Wilson *et al.*, 1995), the West Eifel (Wörner *et al.*, 1986), the Siebengebirge (Wedepohl *et al.*, 1999) and the Westerwald (Haase *et al.*, 2004).

The composition of the shallow lithospheric mantle beneath the Rhenish Massif, and in particular beneath the Eifel, is relatively well known as a result of numerous geochemical and isotopic studies of spinel peridotite xenoliths from the East Eifel and West Eifel volcanic fields (Stosch & Seck, 1980; Stosch & Lugmair, 1986; Witt-Eickschen & Kramm, 1998; Witt-Eickschen *et al.*, 1998, 2003). Most of these peridotitic xenoliths are less radiogenic in Nd and more radiogenic in Sr isotope composition, indicating that such sources cannot represent the source of the nephelinites and basanites. In Pb–Pb isotope space, however, there is broad overlap between the lithospheric spinel peridotites from the East and West Eifel and the nephelinites and basanites from the Hocheifel. Conditions of equilibration of the lithospheric peridotite xenoliths from beneath the Eifel have been estimated to be mostly $<2{\cdot}0$ GPa and $<1100°C$, corresponding to a depth of about 60 km (Witt-Eickschen & Kramm, 1998; Witt-Eickschen *et al.*, 1998, 2003). Therefore, the source of the basanites and nephelinites must be deeper in the mantle; most probably in the asthenosphere. The Sr–Nd–Pb isotope

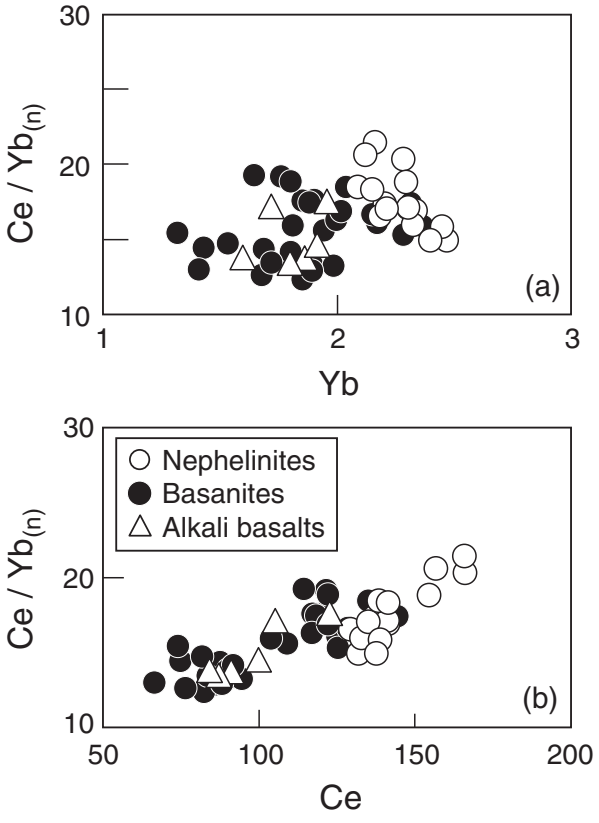

Fig. 14. (a) Chondrite-normalized Ce/Yb vs Yb and (b) chondrite-normalized Ce/Yb(n) vs Ce for mafic alkaline lavas from the Hocheifel. Normalization values are from Boynton (1984).

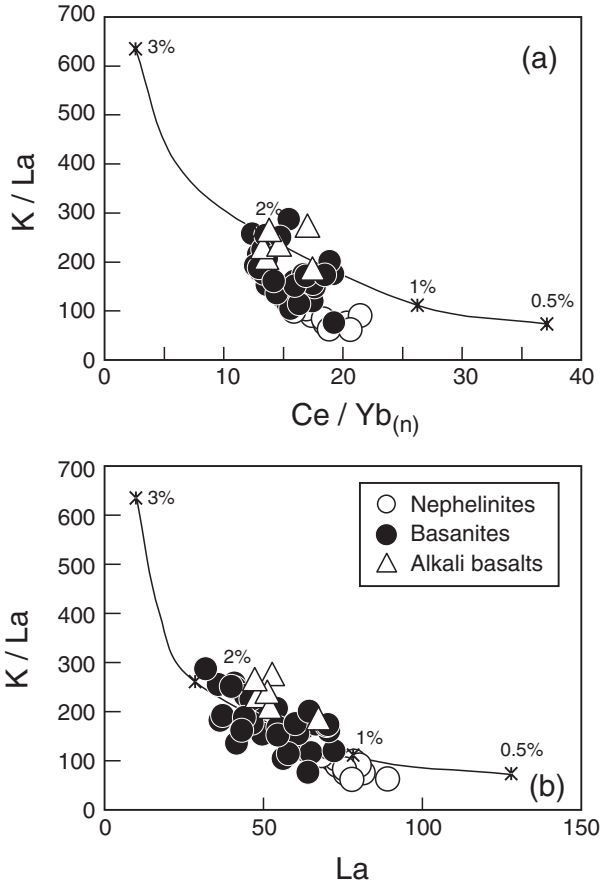

Fig. 15. (a) K/La vs chondrite-normalized Ce/Yb and (b) K/La vs La for mafic alkaline lavas from the Hocheifel. Partial melting curves were calculated using a non-modal, fractional melting model (Shaw, 1970) with the sources and melting modes given in Fig. 12. Source composition has 592 ppm K, 2·1 ppm La, 4·5 ppm Ce and 0·17 ppm Yb, which is the average of 36 peridotite xenoliths from the Hessian Depression (Hartmann & Wedepohl, 1990). Mineral–melt distribution coefficients are from McKenzie & O'Nions (1991), Hart & Dunn (1993), Kelemen *et al.* (1993), Johnston (1994) and LaTourette *et al.* (1995).

composition of the nephelinites and basanites, as well as their similarity to OIB and other primitive alkaline mafic magmas from Central Europe, further suggests that the source of these mafic alkaline lavas is located in the asthenosphere (Wilson & Downes, 1991, 2006), although some workers (Goes *et al.*, 1999; Wedepohl & Baumann, 1999) have suggested a deep mantle origin for the primitive alkaline lavas from Europe. A restricted group of basanites have lower $^{206}Pb/^{204}Pb$ and $^{207}Pb/^{204}Pb$ ratios (Fig. 10). These samples also have lower $^{143}Nd/^{144}Nd$ ratios of <0·51285, relative to the nephelinites and the rest of the basanites, implying a source with lower (U + Th)/Pb and lower $^{147}Sm/^{143}Nd$. This source, with EM affinities, is probably located close to the base of the TBL (thermal boundary layer; McKenzie & Bickle, 1988; Wilson *et al.*, 1995) in the lower lithosphere.

It has been suggested that the Cenozoic volcanism in Central Europe is related to two distinct mantle sources (Wilson & Downes, 1991, 2006; Wilson & Patterson, 2001). One common mantle source [the EAR; European Asthenospheric Reservoir of Cebriá & Wilson (1995) or LVC; Low Velocity Composition of Hoernle *et al.* (1995)] has HIMU-like isotope characteristics and is inferred to be the source of the most primitive Na_2O-rich basalts, whereas another, more enriched mantle source (EM I) contributed to the geochemistry of the more K_2O-rich basalts. The EAR component is probably transported from the deeper mantle to the asthenosphere in small-scale mantle plumelets (Granet *et al.*, 1995), one of which seems to exist beneath the Eifel (Ritter *et al.*, 2001; Keyser *et al.*, 2002). Mixing of partial melts from these two mantle sources may explain the variable Sr–Nd–Pb isotope compositions of the mafic lavas from the CEVP. In addition to the mafic lavas from the Urach–Hegau volcanic field in southern Germany, high $^{206}Pb/^{204}Pb$ ratios (>19·5) have until now been found only in some Quaternary West Eifel lavas (Wörner *et al.*, 1986) and in some mafic lavas from the Westerwald and Siebengebirge

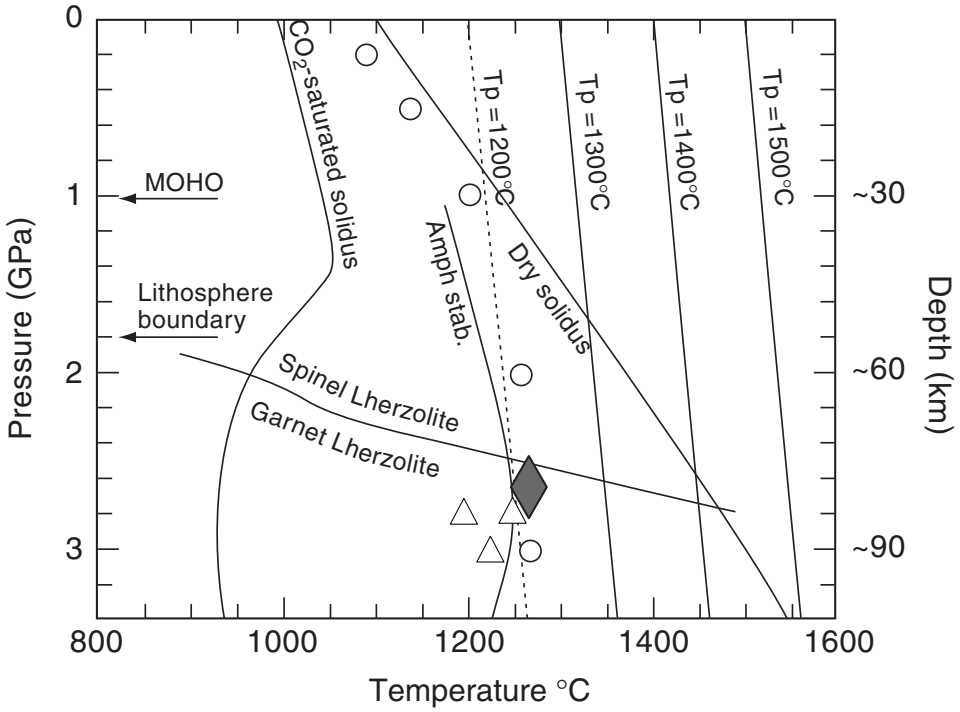

Fig. 16. Pressure–temperature diagram to illustrate the potential source region for mafic alkaline lavas from the Hocheifel. Solidi for dry mantle and CO_2-saturated mantle are from McKenzie & Bickle (1988) and Falloon & Green (1990), respectively. Also shown are adiabats for various mantle potential temperatures. Stability fields for spinel and garnet peridotite and amphibole in upper mantle rocks are from Falloon & Green (1990), Foley (1991) and Robinson & Wood (1998). ○, experimental results of Huckenholz & Gilbert (1980) for the stability of amphibole as a phenocryst phase in basanite and nephelinite from the Hocheifel as discussed in the text. Crustal thickness (Moho) is adopted from Prodehl *et al.* (1992) and the lithosphere–asthenosphere boundary is taken from Babuska & Plomerová (1992). △, experimental results of phlogopite–garnet peridotite melting from Mengel & Green (1986) and Thibault *et al.* (1992). The black diamond approximates the inferred melting region of the Hocheifel lavas.

(Wedepohl & Baumann, 1999; Haase *et al.*, 2004). Excluding the Quaternary West Eifel lavas, the high $^{206}Pb/^{204}Pb$ ratios of the Westerwald, Siebengebirge and Hocheifel lavas probably implies that these volcanic centres were fed from melts of the same (homogeneous?) mantle source during the Tertiary. Haase *et al.* (2004) also observed moderately high $^{206}Pb/^{204}Pb$ ratios up to 19·6 in some mafic lavas from the Westerwald and Siebengebirge, although it is not entirely clear whether these Pb isotope compositions can be interpreted as mixtures of melts of the EAR source (with $^{206}Pb/^{204}Pb$ of ~20, Hoernle *et al.*, 1995) and a more unradiogenic source. The new Hocheifel data presented here, with several mafic lavas having $^{206}Pb/^{204}Pb$ ranging from 19·6 to 20·0, indicate that the EAR component is an important constituent of the upper mantle beneath the Rhenish Massif.

Compositional variations of the Hocheifel magmas with time

To constrain the temporal and compositional variations of the mafic Hocheifel magmas, high-precision Ar–Ar age determinations (Fekiacova, 2004) and geochemical and isotope data from this study were combined. Mafic alkaline volcanism in the Hocheifel started at about 44 Ma, roughly 18 Myr earlier than in the Westerwald and Siebengebirge (Haase *et al.*, 2004). From Fig. 17 it becomes evident that the early mafic alkaline lavas from the Hocheifel have low CaO/Al_2O_3, low La/Yb and high K/La ratios, reflecting a contribution from a source with minor garnet but substantial amounts of a K-bearing mineral, which, in this case, is most probably amphibole. Moreover, these melts have unradiogenic Nd but radiogenic Sr and Pb isotopic compositions and were probably derived by melting of the thermal boundary layer at the base of the lithosphere. The late mafic alkaline lavas have higher CaO/Al_2O_3, higher La/Yb and lower K/La ratios and radiogenic Nd but unradiogenic Sr and Pb isotopic compositions reflecting a dominant contribution from the plume. Together with the compositional and temporal constraints provided by Haase *et al.* (2004), a pulsing of the mantle plume beneath the Rhenish Massif can be suggested. At about 39 Ma, lavas with relatively low $^{206}Pb/^{204}Pb$ ratios (ca. 19·0) were erupted. As noted

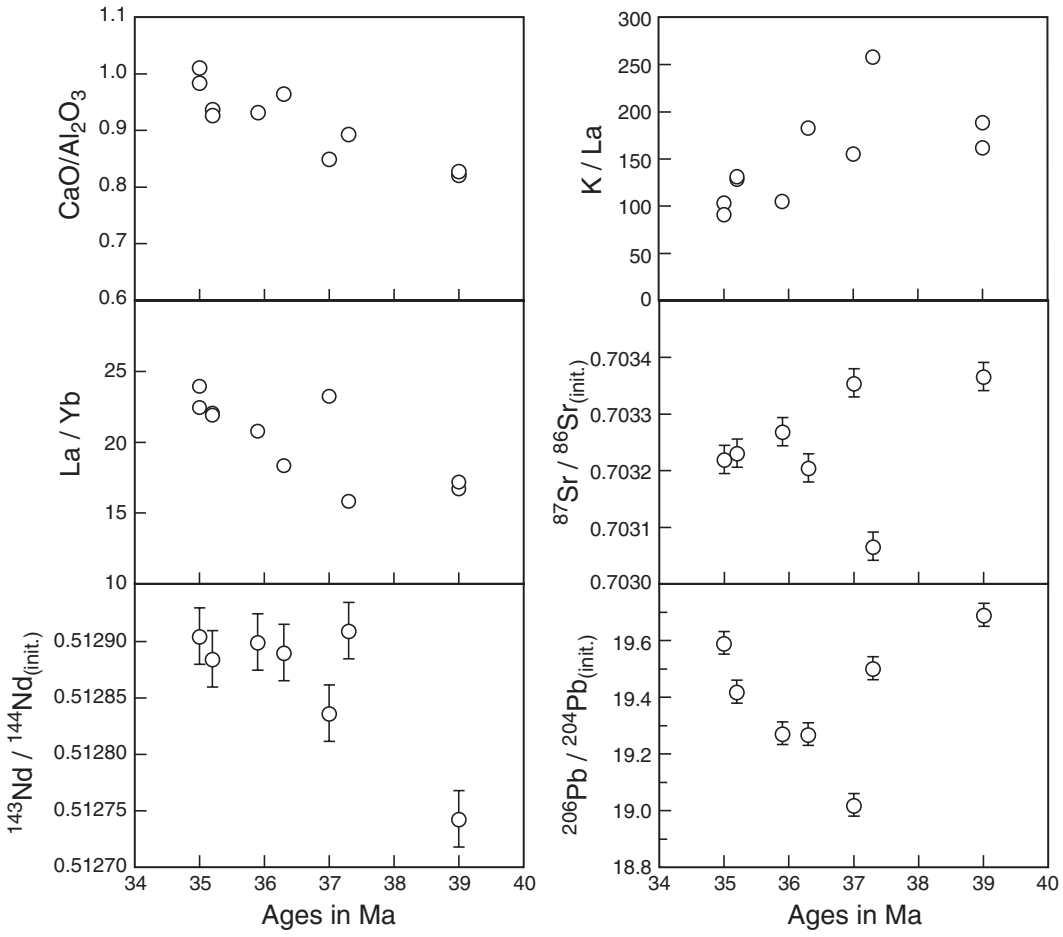

Fig. 17. Temporal variations of chemical and isotopic compositions of the Hocheifel lavas. Ar–Ar ages are from Fekiacova (2004) and include (with decreasing age) Alte Burg (39·0 Ma), Kastelberg (37·3 Ma), Scharfer Kopf (37·0 Ma), Hohe Acht (36·3 Ma), Kapp (35·9 Ma), Neuenahrer Burgberg (35·2 Ma) and Nürburg (35 Ma). (For sample localities see Table 1 and Fig. 1b.)

above, these earlier may reflect a contribution from the thermal boundary layer. Between 37 Ma and 35 Ma, the $^{206}Pb/^{204}Pb$ ratios of the lavas increase to 19·6, suggesting a contribution from the advancing plume. High $^{206}Pb/^{204}Pb$ ratios between 19·3 and 19·7 are also characteristic for the alkaline volcanism of the Siebengebirge and Westerwald, which occurred between ca. 28 Ma and 20 Ma. Between ca. 20 Ma and 10 Ma mafic alkaline lavas from the Vogelsberg and the Hessian Depression display significantly lower $^{206}Pb/^{204}Pb$ ratios between 18·8 and 19·3 Ma, again suggesting a contribution from the thermal boundary layer. In Quaternary times, mafic alkaline magmas from the Eifel display again high $^{206}Pb/^{204}Pb$ ratios of ~19·5, implying reactivation of the plume source. It should be noted that the composition of the younger Hocheifel magmas is similar to that of the Eifel magmas erupted in Quaternary times, implying similar sources for the Tertiary and Quaternary volcanism.

CONCLUSIONS

Geochemical and isotopic studies of Tertiary Hocheifel nephelinites, basanites and alkali basalts provide the following constraints on the evolution of these rocks.

(1) Most of the investigated samples are relatively primitive alkaline rocks, mostly nephelinites and basanites with high Mg-number (>0·60) and high Cr and Ni contents. Some samples are more differentiated magmas that have undergone polybaric fractionation of olivine + clinopyroxene + amphibole ± plagioclase + Fe–Ti oxides.

(2) Incompatible trace element abundances are remarkably similar for nephelinites, basanites and alkali basalts, although alkali basalts tend to have higher Ba/Nb, K/Nb and Ba/La ratios than nephelinites. Sr–Nd–Pb isotope data are broadly similar to other mafic lavas from the CEVP and show overlap for most of the nephelinites, basanites and alkali basalts. One group of basanites has lower $^{206}Pb/^{204}Pb$ (19·13–19·22),

Table 5: Compositions and parameters used for the EC-AFC model calculations (Spera & Bohrson, 2001)

Magma liquidus temperature	1320°C					
Magma temperature t_{m0}	1320°C					
Assimilant liquidus temperature	1100°C					
Country rock temperature t_{a0}	900°C					
Solidus temperature t_s	950°C					
Magma specific heat capacity C_{pm}	1484 J/kg K					
Assimilant specific heat capacity C_{pa}	1388 J/kg K					
Crystallization enthalpy	396 000 J/kg					
Fusion enthalpy	354 000 J/kg					
Equilibration temperature	980°C					
	Sr (ppm)	Nd (ppm)	Pb (ppm)	K (ppm)	Nb (ppm)	Zr (ppm)
Magma HEJ 53	723	39·2	10	10790	59	198
Bulk distribution coefficient D_0	0·1	0·1	0·1	0·1	0·1	0·1
Enthalpy	0	0	0	0	0	0
Assimilant S 32	1325	36·9	4·57	4100	6	70
Bulk distribution coefficient D_0	0·5	0·25	0·1	0·1	0·1	0·1
Enthalpy	0	0	0	0	0	0
	$^{87}Sr/^{86}Sr$	$^{143}Nd/^{144}Nd$	$^{206}Pb/^{204}Pb$			
Magma HEJ 53	0·703282	0·512821	19·53			
Assimilant S 32	0·70948	0·512198	19·04			

t_{m0}, initial magma temperature; t_{a0}, initial country rock temperature. Assimilant S 32 is a mafic granulite xenolith (Stosch & Lugmair, 1984; Rudnick & Goldstein, 1990).

$^{207}Pb/^{204}Pb$ (15·46–15·50) and $^{143}Nd/^{144}Nd$ ratios (0·51276–0·51285) than the rest of the basanites and nephelinites, which have more radiogenic Pb and Nd isotope compositions. These features imply the existence of at least two different mantle sources in the petrogenesis of the mafic Hocheifel lavas. One source is similar to an asthenospheric OIB-type source (EAR: Cebriá & Wilson, 1995; LVC: Hoernle *et al.*, 1995), whereas the source of the basanites with unradiogenic Pb and Nd isotope compositions could be a part of the TBL, located at the base of the subcontinental lithospheric mantle. The more differentiated samples have probably assimilated material from the lower crust similar in composition to the granulite xenoliths described from the Eifel.

(3) Variations in REE abundances are compatible with mixing of melt fractions from garnet peridotite with melt fractions from spinel peridotite, both containing residual amphibole. The incompatible trace element enriched, but isotopically depleted nature of the basalts requires a recently enriched mantle source.

(4) The petrogenetic model for the Hocheifel basalts implies the existence of melts from sub-lithospheric sources and melts from the base of the lithospheric mantle. Old, depleted subcontinental lithospheric mantle is too dry to yield significant quantities of melt, even when heated by an upwelling mantle plume; consequently, infiltrating fluids and melts from such plumes are required to metasomatize the base of the subcontinental lithospheric mantle. During ascent, partial melts from the upwelling plume heat and partially melt the metasomatized subcontinental lithospheric mantle by dehydration melting (Gallagher & Hawkesworth, 1992). If the overlying mantle lithosphere and crust is not drastically weakened, the geochemistry and isotope composition of the first small-degree partial melts should reflect that of the subcontinental lithospheric mantle, whereas the composition of the later, larger-degree partial melts may carry the signature of the plume itself. Melt generation at the base of the subcontinental lithospheric mantle can, therefore, lead to structural weakening of the lithosphere and can also promote thermal erosion of the base of the lithosphere. Substantial amounts of melt can be generated within the lithosphere for β factors (the ratio of unstretched to stretched lithosphere, McKenzie & Bickle, 1988) $<1{\cdot}2$ (Gallagher & Hawkesworth, 1992). In regions with β factors $>1{\cdot}3$ for a 100 km thick lithosphere, the upwelling plume will melt to increasingly larger degrees and magmas derived from the plume will dominate over those derived from the SCLM. In the model of Hawkesworth & Gallagher (1993), a sequence of events is predicted. The first melts come from the lower part of the thermal boundary layer where low-degree partial melts from the advancing plume freeze and precondition the base of the lithosphere. This event is

followed by the generation of melts with a plume signature. Such features are consistent with the temporal and isotopic constraints provided by the mafic lavas from the Hocheifel. The minimum thickness of the lithosphere prior to the Cenozoic volcanism is estimated to be ~100 km (Babuska & Plomerová, 1988). Tomographic studies suggest uplift of the lithosphere–asthenosphere boundary to a minimum depth of 50 km beneath the Eifel area (Panza *et al.*, 1980), suggesting a β factor of ~2·0. At these ratios of unstretched to stretched lithosphere, partial melting in the asthenosphere starts at an initial mantle temperature of ~1300°C (Hawkesworth & Gallagher, 1993), which is compatible with the estimates from this study.

ACKNOWLEDGEMENTS

S. Hoernes (Universität Bonn) kindly provided XRF analysis, and A. W. Hofmann (Max-Planck-Insitut für Chemie, Mainz) is thanked for hospitality and for giving access to the mass spectrometry facilities. Considerable thanks go to Iris Bambach (Mainz) for her patience during managing of the line drawings. We appreciate the help of D. Neuhäuser, U. Poller, W. Todt and P. Maissenbacher during the second author's stay in Mainz. Constructive and unbiased reviews were provided by J.-M. Cebriá, M. Wilson and G. Wörner and are highly appreciated. Finally, we would like to thank M. Wilson for improving the style of the manuscript and for providing us with a preprint of the Wilson & Downes (2006) paper about Quaternary to Tertiary magmatism in Europe. This study was largely funded through grants from the Philipps-Universität (Marburg) to C.J.

REFERENCES

Alibert, C., Leterrier, J., Panasiuk, M. & Zimmermann, J. L. (1987). Trace and isotope geochemistry of the alkaline Tertiary volcanism in southwest Poland. *Lithos* **20**, 311–321.

Arndt, N. T. & Christensen, U. (1992). The role of lithospheric mantle in continental flood volcanism: thermal and geochemical constraints. *Journal of Geophysical Research* **97**, 10967–10981.

Babuska, V. & Plomerová, J. (1988). Subcrustal continental lithosphere: a model of its thickness and anisotropic structure. *Physics of the Earth and Planetary Interiors* **51**, 130–132.

Baker, J. A., Menzies, M. A., Thirlwall, M. F. & MacPherson, C. G. (1997). Petrogenesis of Quaternary intraplate volcanism, Sana'a, Yemen: implications for plume–lithosphere interaction and polybaric melt hybridization. *Journal of Petrology* **38**, 1359–1390.

Blusztajn, J. & Hart, S. R. (1989). Sr, Nd, and Pb isotopic character of Tertiary basalts from southwest Poland. *Geochimica et Cosmochimica Acta* **53**, 2689–2696.

Blusztajn, J. & Hegner, E. (2002). Osmium isotopic systematics of melilitites from the Tertiary Central European Volcanic province in SW Germany. *Chemical Geology* **189**, 91–103.

Bogaard, P. F.J. & Wörner, G. (2003). Petrogenesis of basanitic to tholeiitic volcanic rocks from the Miocene Vogelsberg, Central Germany. *Journal of Petrology* **44**, 569–602.

Boynton, W. V. (1984). Geochemistry of the rare earth elements: meteorite studies. In: Henderson, P. (ed.) *Rare Earth Element Geochemistry*. Amsterdam: Elsevier, pp. 63–114.

Bradshaw, T. K., Hawkesworth, C. J. & Gallagher, K. (1993). Basaltic volcanism in the Southern Basin and Range: no role for a mantle plume. *Earth and Planetary Science Letters* **116**, 45–62.

Brey, G. & Green, D. H. (1977). Systematic study of liquidus phase relations in olivine melilitite + H_2O + CO_2 at high pressures and petrogenesis of an olivine melilitite magma. *Contributions to Mineralogy and Petrology* **61**, 141–162.

Cameron, A. E., Smith, D. H. & Walker, R. L. (1969). Mass spectrometry of nanogram-size samples of lead. *Analytical Chemistry* **41**, 525–526.

Cantarel, P. & Lippolt, H. J. (1977). Age and sequence of Tertiary volcanism in the Hocheifel area, Germany. *Neues Jahrbuch für Geologie und Paläontologie, Monatshefte* **1977**, 600–612.

Cebriá, J. M. & Wilson, M. (1995). Cenozoic mafic magmatism in Western/Central Europe: a common European asthenospheric reservoir? *Terra Nova, Abstracts Supplement* **7**, 162.

Downes, H. (1984). Sr and Nd isotope geochemistry of coexisting alkaline magma series, Cantal, Massif Central, France. *Earth and Planetary Science Letters* **69**, 321–334.

Downes, H., Seghedi, I., Szakacs, A., Dobosi, G., James, D. E., Vasselli, O., Rigby, I. J., Ingram, G. A., Rex, D. & Pecskay, Z. (1995). Petrology and geochemistry of late Tertiary/Quaternary mafic alkaline volcanism in Romania. *Lithos* **35**, 65–81.

Duda, A. & Schmincke, H. U. (1985). Polybaric differentiation of alkali basaltic magma: evidence from green-core clinopyroxenes (Eifel, Germany). *Contributions to Mineralogy and Petrology* **91**, 340–351.

Ellam, R. M. & Cox, K. G. (1991). An interpretation of Karoo picrite basalts in terms of interaction between asthenosphere magmas and the mantle lithosphere. *Earth and Planetary Science Letters* **105**, 330–342.

Embey-Isztin, E., Downes, H., James, D. E., Upton, B. G. J., Dobosi, G., Ingram, G. A., Harmon, R. S. & Scharbert, H. G. (1993). The petrogenesis of Pliocene alkaline volcanic rocks from the Pannonian Basin, Eastern Central Europe. *Journal of Petrology* **34**, 317–343.

Engelhardt, H. J. (1990). TUC-Referenzproben in Geochemie und Umweltanalytik. *Mitteilungsblatt TU Clausthal* **70**, 26–28.

Falloon, T. J. & Green, D. H. (1990). Solidus of carbonated fertile peridotite under fluid-saturated conditions. *Geology* **18**, 195–199.

Fekiacova, Z. (2004). Geochronology, geochemistry and isotopic composition of the volcanic rocks from oceanic (Hawaii) and continental (Eifel) intra-plate environments. Ph.D. dissertation, University of Mainz, 109 pp.

Fekiacova, Z., Mertz, D. F. & Renne, P. (2003). Geodynamic setting of the Hocheifel volcanism, western Germany. *Geophysical Research Abstracts* **5**, 10355.

Foley, S. (1991). High-pressure stability of the fluor- and hydroxy-endmembers of pargasite and K-richterite. *Geochimica et Cosmochimica Acta* **55**, 2689–2694.

Frey, F. A., Green, D. H. & Roy, S. D. (1978). Integrated models of basalt petrogenesis: a study of quartz tholeiites to olivine melilitites from South Eastern Australia utilizing geochemical and experimental petrological data. *Journal of Petrology* **19**, 463–513.

Gallagher, K. & Hawkesworth, C. J. (1992). Dehydration melting and the generation of continental flood basalts. *Nature* **358**, 57–59.

Goes, S., Spakman, H. & Bijwaard, H. (1999). A lower mantle source for Central European volcanism. *Science* **286**, 1928–1931.

Govindaraju, K. (ed.) (1994). Compilation of working values ansd sample description for 383 geostandards. *Geostandards Newsletter* **17**, 158 pp.

Granet, M., Wilson, M. & Achauer, U. (1995). Imaging a mantle plume beneath the French Massif Central. *Earth and Planetary Science Letters* **136**, 281–296.

Haase, K. M., Goldschmidt, B. & Garbe-Schönberg, D. (2004). Petrogenesis of Tertiary continental intra-plate lavas from the Westerwald region, Germany. *Journal of Petrology* **45**, 883–905.

Harangi, S. (1994). Geochemistry and petrogenesis of the early Cretaceous continental rift-type volcanic rocks of the Mecsek Mountains, South Hungary. *Lithos* **33**, 303–321.

Hart, S. R. (1984). A large-scale isotope anomaly in the southern hemisphere mantle. *Nature* **309**, 753–757.

Hart, S. R. & Davis, K. E. (1978). Nickel partitioning between olivine and silicate melt. *Earth and Planetary Science Letters* **40**, 203–219.

Hart, S. R. & Dunn, T. (1993). Experimental clinopyroxene/melt partitioning of 24 trace elements. *Contributions to Mioneralogy and Petrology* **113**, 1–8.

Hart, W. K., Carlson, R. W. & Shirey, S. B. (1997). Radiogenic Os in primitive basalts from the northwestern U.S.A.: implications for petrogenesis. *Earth and Planetary Science Letters* **150**, 103–116.

Hartmann, G. & Wedepohl, K. H. (1990). Metasomatically altered peridotite xenoliths from the Hessian Depression (Northwest Germany). *Geochimica et Cosmochimica Acta* **54**, 71–86.

Hawkesworth, C. J. & Gallagher, K. (1993). Mantle hotspots, plumes and regional tectonics as causes of intraplate magmatism. *Terra Nova* **5**, 552–559.

Hawkesworth, C. J., Kempton, P. D., Rogers, N. W., Ellam, R. M. & van Calsteren, P. W. (1990). Continental mantle lithosphere and shallow level enrichment processes in the Earth's mantle. *Earth and Planetary Science Letters* **96**, 256–268.

Hegner, E., Walter, H. J. & Satir, M. (1995). Pb–Sr–Nd isotopic compositions and trace element geochemistry of megacrysts and melilitites from the Tertiary Urach volcanic field: source composition of small volume melts under SW Germany. *Contributions to Mineralogy and Petrology* **122**, 322–335.

Heinrichs, H. & Herrmann, A. G. (1990). *Praktikum der Analytischen Geochemie*. Berlin: Springer.

Hirose, K. (1997). Partial melt compositions of carbonated peridotite at 3 GPa and role of CO_2 in alkali-basalt magma generation. *Geophysical Research Letters* **24**, 2837–2840.

Hoernle, K., Zhang, Y.-S. & Graham, D. (1995). Seismic and geochemical evidence for large-scale mantle upwelling beneath the eastern Atlantic and western and central Europe. *Nature* **374**, 34–39.

Huckenholz, H. G. & Büchel, G. (1988). Tertiärer Vulkanismus der Hocheifel. *Fortschritte der Mineralogie* **66**(Bh2), 43–82.

Huckenholz, H. G. & Gilbert, M. C. (1984). Stabilität von Ca-Amphibol in Alkalibasalten der Hocheifel. *Fortschritte der Mineralogie* **62**(Bh1), 106–107.

Huckenholz, H. G., Kunzmann, T. & Spicker, G. (1988). Stability of titanian magnesio-hastingsite and its breakdown to rhönite-bearing assemblage. *Terra Cognita* **8**, 66.

Huppert, H. E. & Sparks, R. S. J. (1988). The fluid dynamics of a basaltic magma chamber replenished by influx of hot, dense ultrabasic magma. *Contributions to Mineralogy and Petrology* **75**, 279–289.

Jaques, A. L. & Green, D. H. (1980). Anhydrous melting of peridotite at 0–15 Kb pressure and the genesis of tholeiitic basalts. *Contributions to Mineralogy and Petrology* **73**, 287–310.

Johnson, K. T. M. (1998). Experimental determination of partition coefficients for rare earth and high-field-strength elements between clinopyroxene, garnet, and basaltic melt at high pressures. *Contributions to Mineralogy and Petrology* **133**, 60–68.

Jung, S. & Hoernes, S. (2000). The major- and trace element and isotope (Sr, Nd, O) geochemistry of Cenozoic alkaline rift-type volcanic rocks from the Rhön area (central Germany): petrology, mantle source characteristics and implications for asthenosphere–lithosphere interactions. *Journal of Volcanology and Geothermal Research* **99**, 27–53.

Jung, S. & Masberg, P. (1998). Major- and trace element systematics and isotope geochemistry of Cenozoic mafic volcanic rocks from the Vogelsberg (Central Germany)—constraints on the origin of continental alkaline and tholeiitic basalts and their mantle sources. *Journal of Volcanology and Geothermal Research* **86**, 151–177.

Jung, S., Pfänder, J. A., Brügmann, G. & Stracke A. (2006).Sources of primitive alkaline volcanic rocks from the Central European Volcanic Province (Rhön, Germany) inferred from Hf, Os and Pb isotopes. *Contributions to Mineralogy and Petrology* (in press).

Kelemen, P. B., Shimizu, N. & Dunn, T. (1993). Relative depletion of niobium in some arc magmas and the continental crust: partitioning of K, Nb, La and Ce during melt/rock reaction in the upper mantle. *Earth and Planetary Science Letters* **120**, 111–134.

Keyser, M., Ritter, J. R. R. & Jordan, M. (2002). 3D shear-wave velocity structure of the Eifel plume, Germany. *Earth and Planetary Science Letters* **203**, 59–82.

Kushiro, I. (1996). Partial melting of a fertile mantle peridotite at high pressures: an experimental study using aggregates of diamond. In: Basu, A. & Hart, S. R. (eds) *Earth Processes: Reading the Isotopic Code. Geophysical Monograph, American Geophysical Union* **95**, 109–122.

LaTourrette, T., Hervig, R. L. & Holloway, J. R. (1995). Trace element partitioning between amphibole, phlogopite, and basanite melt. *Earth and Planetary Science Letters* **135**, 13–30.

Le Bas, M. J. (1989). Nephelinitic and basanitic rocks. *Journal of Petrology* **30**, 1299–1312.

Le Bas, M. J., Le Maitre, R. W., Streckeisen, A. & Zanettin, B. (1986). A chemical classification of volcanic rocks based on the total alkali–silica diagram. *Journal of Petrology* **27**, 745–750.

Lechler, P. J. & Desilets, M. O. (1987). A review of the use of loss on ignition as a measurement of total volatiles in whole rock analysis. *Chemical Geology* **63**, 341–344.

Lippolt, H. J. (1982). K/Ar age determinations and the correlation of Tertiary volcanic activity in Central Europe. *Geologisches Jahrbuch Hannover* **D 52**, 113–135.

Loock, G., Stosch, H.-G. & Seck, H. A. (1990). Granulite facies lower crustal xenoliths from the Eifel, West Germany: petrological and geochemical aspects. *Contributions to Mineralogy and Petrology* **195**, 25–41.

Mattinson, J. M. (1986). Geochronology of high-pressure–low temperature Franciscan metabasites. A new approach using the U–Pb system. *Geological Society of America, Memoirs* **164**, 95–105.

McKenzie, D. & Bickle, M. J. (1988). The volume and composition of melt generated by extension of lithosphere. *Journal of Petrology* **29**, 625–679.

McKenzie, D. & O'Nions, R. K. (1991). Partial melt distributions from inversion of rare earth element concentrations. *Journal of Petrology* **32**, 1021–1091.

Mengel, K. & Green, D. H. (1986). Stability of amphibole and phlogopite in metasomatized peridotite under water-saturated and water-undersaturated conditions. In: Ross, J., Jaques, A. L., Ferguson, J., Green, D. H., O'Reilly, S. Y., Danchin, R. V. & Janse, A. J. A. (eds) *Kimberlites and Related Rocks 1*. Oxford: Blackwell Scientific, pp. 571–581.

Mengel, K., Sachs, P. M., Stosch, H. G., Wörner, G. & Loock, G. (1991). Crustal xenoliths from Cenozoic volcanic fields of West Germany: implications for structure and composition of the crust. *Tectonophysics* **195**, 271–289.

Mertes, H. & Schmincke, H. U. (1983). Mafic potassic lavas of the Quaternary West Eifel volcanic field. I. Major and trace elements. *Contributions to Mineralogy and Petrology* **89**, 330–345.

Mysen, B. O. & Kushiro, I. (1977). Compositional variations of coexisting phases with degree of melting of peridotite in the upper mantle. *American Mineralogist* **62**, 843–865.

Panza, G. F., Mueller, S. & Calcagnile, G. (1980). The gross features of the lithosphere–asthenosphere system in Europe from seismic surface waves and body waves. *Paleophysics* **118**, 1209–1213.

Prodehl, C., Müller, S., Glahn, A., Gutsher, M. & Haak, V. (1992). Lithosphere cross-section of the European rift system. In: Ziegler, P. A. (ed.) *Geodynamics of Fifting, 1. Case Histories on Rifts: Europe and Asia. Tectonophysics* **208**, 113–138.

Rapp, R. P., Watson, E. B. & Miller, C. F. (1991). Partial melting of amphibolite/eclogite and the origin of Archean trondhjemites and tonalites. *Precambrian Research* **51**, 1–25.

Reiners, P. W., Nelson, B. K. & Ghiorso, M. S. (1995). Assimilation of felsic crust by basaltic magma: thermal limits and extents of crustal contamination of mantle-derived magmas. *Geology* **23**, 563–566.

Ritter, J. R. R., Jordan, M., Christensen, U. R. & Achauer, U. (2001). A mantle plume below the Eifel volcanic fields, Germany. *Earth and Planetary Science Letters* **186**, 7–14.

Robinson, J. A. C. & Wood, B. J. (1998). The depth of the spinel to garnet transition at the peridotite solidus. *Earth and Planetary Science Letters* **164**, 277–284.

Rudnick, R. L. & Fountain, D. M. (1995). Nature and composition of the continental crust: a lower crustal perspective. *Reviews in Geophysics* **33**, 267–309.

Rudnick, R. & Goldstein, S. L. (1990). The Pb isotopic evolution of lower crustal xenoliths and the evolution of lower crustal Pb. *Earth and Planetary Science Letters* **98**, 192–207.

Sachs, P. M. & Hansteen, T. H. (2000). Pleistocene underplating and metasomatism of the lower continental crust: a xenolith study. *Journal of Petrology* **41**, 331–356.

Schmincke, H. U., Lorenz, V. & Seck, H. A. (1983). Quaternary Eifel volcanic fields. In: Fuchs, K., von Gehlen, K., Maelzer, H., Murawski, H. & Semmel, A. (eds) *Plateau Uplift*. Berlin: Springer, pp. 139–151.

Schreiber, U. & Rotsch, S. (1998). Cenozoic block rotation according to a conjugate shear system in central Europe—indications from paleomagnetic measurements. *Tectonophysics* **299**, 111–142.

Shaw, D. M. (1970). Trace element fractionation during anatexis. *Geochimica et Cosmochimica Acta* **34**, 237–243.

Spera, F. J. & Bohrson, W. A. (2001). Energy-constrained open-system magmatic processes; I, General model and energy-constrained assimilation and fractional crystallization (EC-AFC) formulation. *Journal of Petrology* **42**(5), 999–1018.

Stosch, H.-G. & Lugmair, G. W. (1984). Evolution of the lower continental crust: granulite facies xenoliths from the Eifel, West Germany. *Nature* **311**, 368–370.

Stosch, H.-G. & Lugmair, G. W. (1986). Trace element and Sr and Nd isotope geochemistry of peridotite xenoliths from the Eifel (West Germany) and their bearing on the evolution of the subcontinental lithosphere. *Earth and Planetary Science Letters* **80**, 281–298.

Stosch, H.-G. & Seck, H. A. (1980). Geochemistry and mineralogy of two spinel peridotite suites from Dreiser Weiher, West Germany. *Geochimica et Cosmochimica Acta* **44**, 457–470.

Stosch, H.-G., Lugmair, G. W. & Seck, H. A. (1986). Geochemistry of granulite-facies lower crustal xenoliths: implications for the geological history of the lower continental crust below the Eifel, West Germany. In: Dawson, J. B., Carswell, D. A., Hall, J. & Wedepohl, K. H. (eds) *The Nature of the Lower Continental Crust. Geological Society, London, Special Publications* **24**, 309–317.

Stosch, H.-G., Schmucker, A. & Reys, C. (1992). The nature and geological history of the deep crust under the Eifel, Germany. *Terra Nova* **4**, 53–62.

Sun, S.-S. & McDonough, W.F. (1989). Chemical and isotopic systematics of oceanic basalts: implications for mantle composition and processes. In: Saunders, A. D. & Norry, M. J. (eds) *Magmatism in the Ocean Basins. Geological Society Special Publications* **42**, 313–345.

Taylor, S. R. & McLennan, S. M. (1985). *The Continental Crust: its Composition and Evolution*. Oxford: Blackwell Scientific, 312 pp.

Thibault, Y., Edgar, A. D. & Lloyd, F. E. (1992). Experimental investigation of melts from a carbonated phlogopite lherzolite: implications for metasomatism in the continental lithosphere. *American Mineralogist* **77**, 784–794.

Thirlwall, M. F., Upton, B. G. J. & Jenkins, C. (1994). Interaction between continental lithosphere and the Iceland plume—Sr–Nd–Pb isotope chemistry of Tertiary basalts, NE Greenland. *Journal of Petrology* **35**, 839–897.

Vogel, W. & Kuipers, G. (1987). A pre-calibrated program for geological applications. *Phillips New Developments in X-Ray Spectrometry* **11**, 2–8.

Weaver, B. L. (1991). The origin of ocean island basalts endmember compositions: trace element and isotopic constraints. *Earth and Planetary Science Letters* **104**, 381–397.

Wedepohl, K. H. (1985). Origin of the Tertiary basaltic volcanism in the Northern Hessian depression. *Contributions to Mineralogy and Petrology* **89**, 122–143.

Wedepohl, K. H. & Baumann, A. (1999). Central European Cenozoic plume volcanism with OIB characteristics and indications of lower mantle source. *Contributions to Mineralogy and Petrology* **136**, 225–239.

Wedepohl, K. H., Gohn, E. & Hartmann, G. (1994). Cenozoic alkali basaltic magmas of western Germany and their products of differentiation. *Contributions to Mineralogy and Petrology* **115**, 253–278.

White, R. & McKenzie, D. (1989). Magmatism at rift zones: the generation of volcanic continental margins and flood basalts. *Journal of Geophysical Research* **94**, 7685–7729.

Wilson, M. & Downes, H. (1991). Tertiary–Quarternary extension-related alkaline magmatism in Western and Central Europe. *Journal of Petrology* **32**, 811–849.

Wilson, M. & Downes, H. (2006). Tertiary–Quaternary intra-plate magmatism in Europe and its relationship to mantle dynamics. In: Stephenson, R. A. & Gee, D. (eds) *European Lithosphere Dynamics. Geological Society of London, Memoirs* (in press).

Wilson, M. & Patterson, R. (2001). Intra-plate magmatism related to hot fingers in the upper mantle: evidence from the Tertiary–Quarternary volcanic province of western and central Europe. In: Ernst, R. & Buchan, K. (eds) *Mantle Plumes: their Identification through Time. Geological Society of America, Special Papers* **352**, 37–58.

Wilson, M., Downes, H. & Cebriá, J.-M. (1995*a*). Contrasting fractionation trends in coexisting continental alkaline magma series; Cantal, Massif Central, France. *Journal of Petrology* **36**, 1729–1753.

Wilson, M., Rosenbaum, J. M. & Dunworth, E. A. (1995*b*). Melilitites: partial melts of the thermal boundary layer? *Contributions to Mineralogy and Petrology* **119**, 181–196.

Witt-Eickschen, G. & Kramm, U. (1997). Mantle upwelling and metasomatism beneath Central Europe: geochemical and isotopic constraints from mantle xenoliths from the Rhön (Germany). *Journal of Petrology* **38**, 479–493.

Witt-Eickschen, G. & Kramm, U. (1998). Evidence for the multiple stage evolution of the subcontinental lithospheric mantle beneath the Eifel (Germany) from pyroxenite and composite pyroxenite/peridotite xenoliths. *Contributions to Mineralogy and Petrology* **131**, 258–272.

Witt-Eickschen, G., Kaminsky, W., Kramm, U. & Harte, B. (1998). The nature of young vein metasomatism in the lithosphere of the

West Eifel (Germany): geochemical and isotopic constraints from composite mantle xenoliths from the Meerfelder Maar. *Journal of Petrology* **39**, 155–185.

Witt-Eickschen, G., Seck, H. A., Mezger, K., Eggins, S. M. & Altherr, R. (2003). Lithospheric mantle evolution beneath the Eifel (Germany): constraints from Sr–Nd–Pb isotopes and trace element abundances in spinel peridotite and pyroxenite xenoliths. *Journal of Petrology* **44**, 1077–1095.

Wörner, G., Zindler, A., Staudigel, H. & Schmincke, H. U. (1986). Sr, Nd, and Pb isotope geochemistry of Tertiary and Quarternary alkaline volcanics from West Germany. *Earth and Planetary Science Letters* **79**, 107–119.

Ziegler, P. A. (1992). European Cenozoic rift system. *Tectonophysics* **208**, 91–111.

Zindler, A. & Hart, S. (1986). Chemical geodynamics. *Annual Review of Earth and Planetary Sciences* **14**, 493–571.